Monolithic and staggered solution strategies for constrained mechanical systems in optimal control problems

Ashutosh Bijalwan[1], Simeon Schneider[2], Peter Betsch[2], José J Muñoz[1,3,4]

[1] Centre Internacional de Mètodes Numèrics en Enginyeria (CIMNE), 08034 Barcelona, Spain.
[2]Institute of Mechanics, Karlsruhe Institute of Technology (KIT), 76131 Karlsruhe, Germany.
[3]Universitat Politècnica de Catalunya (UPC), 08034 Barcelona, Spain.
[4]Institut de Matemàtiques de la UPC -BarcelonaTech (IMTech), 08028 Barcelona, Spain.

Abstract

[Abstract]This paper deals with the optimal control of constrained mechanical systems, with potential additional kinematic constraints at the final time. Correspondingly, the equations of motion of the underlying mechanical system assume the form of differential-algebraic equations with end constraints. The proposed discretisation of the optimality conditions yields a scheme which is capable to preserve control angular momentum maps resulting from the rotational symmetry of the underlying optimal control problem. The numerical solution of the discretised system is first tested with two solution strategies: monolithic and staggered approaches, and then also solved with hybrid approaches, which combine salient features of each individual strategy. The monolithic strategy solves all the optimality conditions for all time-steps as a single system of non-linear equations, and relies on a Newton-Raphson scheme, which guarantees quadratic rates of convergence in the vicinity of the optimal solution trajectory. The staggered strategy is based on the Forward-Backward Sweep Method (FBSM), where state and adjoint equations are solved separately, and the control equations provides an update of the control variables, which we here achieve with also a Newton-Raphson scheme. The proposed hybrid strategies combine the advantages of a conventional gradient-based FBSM with the individual Newton-based solution procedures once the solution is close to the optimal trajectory. The strategies are developed and compared through three representative numerical examples, which show that all schemes yield very similar solutions. However, the hybrid approaches becomes more advantageous with regard to the computation time when the time-step decreases or the size of the problem increases.

Keywords: Mechanical control system, differential-algebraic equations (DAEs), conservation laws, symplectic Euler scheme, staggered solver, FBSM.

1 Introduction

Optimal control problems are based on state equations either in the form of ordinary differential equations (ODEs), or differential-algebraic equations (DAEs), and have a wide range of applications such as minimal effort manoeuvring of industrial robots, minimal fuel landing on the moon's surface or trajectory planning, among others [9, 15, 21]. Concerning the state equations of controlled mechanical systems one has the option to use either minimal coordinates or redundant coordinates. While minimal coordinates lead to equations of motion in the form of ODEs, redundant coordinates yield DAEs. However, the choice of minimal coordinates is not always possible, whereas redundant coordinates provide a general and versatile way to describe constrained mechanical systems in a singularity-free manner [7]. Although the index-3 DAEs governing the motion of mechanical systems subject to holonomic constraints are prone to numerical ill-conditioning, one may apply index-reduction procedures such as the Gear−Gupta−Leimkuhler (GGL) stablisation to form equivalent index-2 DAEs [2, 20, 21, 35, 36]. However, such a procedure introduces additional variables and thus increases the size of the optimal control problem [39, 46]. Alternatively, null-space projection [6, 31] can be used to formulate the optimal control of constrained mechanical systems [8, 26, 27, 28, 41]. Here, we are persuaded by the index-3 DAE formulation since it provides the most natural and straightforward representation of a constrained mechanical system.

Depending on the order of optimisation and discretisation, solution approaches for optimal control problems are classified into the indirect and direct methods, also known as *optimise then discretise* and *discretise then optimise*, respectively [9, 21]. Under certain circumstances [4, 38, 40], both approaches are equivalent as they form identical nonlinear programming problems (NLP).

In the indirect approach, the first-order necessary conditions of optimality are obtained from the Pontryagin Maximum Principle which gives rise to Euler-Lagrange equations as a system of DAEs along with two-point boundary conditions. Correspondingly, the optimal control problem is governed by a Hamiltonian boundary value problem which implies the symplectic property of the solution [4, 13, 19, 23, 40, 43]. Additionally, when optimal control problems have time translation and rotational symmetries, the control Hamiltonian and the control angular momentum are preserved along the optimal trajectories [4, 5, 14, 40].

Thus it is desirable to employ a numerical integrator which preserves the geometric structure of the underlying optimal control problem. This observation led to two important classes of conserving discretisation methods for the underlying Hamiltonian boundary value problem. Firstly, the indirect Hamiltonian preserving method proposed by [11, 12], which yields a second-order scheme. Secondly, symplectic methods which have been developed in the framework of optimal control problems [4, 12, 19, 34]. In the present work we propose a direct symplectic method which can be viewed as extension of the ODE-based scheme [4] to the present case of index-3 state DAEs [40]. In particular, we show that the proposed scheme is capable to preserve control angular momentum maps associated with rotational symmetries of the underlying optimal control problem.

Numerical solution procedures for NLP can be classified into monolithic and staggered methods. The monolithic approach solves the discrete optimality conditions consisting of state, adjoint, and control equations all at once. For this purpose, Newton-based methods can be employed in a straightforward way to achieve quadratic rates of convergence in the vicinity of the optimal solution [9, 11, 19, 45]. In contrast to that, conventional staggered solution approaches such as the Forward-Backward Sweep Methods (FBSM), rely on the forward/backward integration of the state/adjoint equations in conjunction with a gradient-based update procedure for the controls [18, 25, 29, 32]. One major drawback of the staggered approach is that convergence becomes often extremely slow in the vicinity of the optimal solution [29, 32, 33]. In the quest for a more efficient implementation of a staggered solver, we propose a new variant, which resorts to Newton-based updates and restores the quadratic rates of convergence in the vicinity of the optimal solution.

The success of a FSBM relies on the provision of appropriate initial conditions for the state variables and final conditions for the adjoint variables. However, optimal control problems with prescribed initial and final states lead to no boundary conditions for the adjoint variables, and penalty-based formulations for the enforcement of the final states are the only available choice [25, 32]. Recently, a method that accounts for terminal state constraints in the context of the adjoint method for time-optimal control problems with state ODEs has been proposed [18]. In the same spirit, we newly devise a staggered FBSM solution procedure for optimal control problems subjected to index-3 state DAEs with prescribed initial and final states.

It is evident that for moderate-size NLP, Newton-based solvers exhibit good convergence properties provided a good initial guess is utilised. Unarguably, the numerical solution of optimal control problems is a challenging task and the success of the solver heavily relies on the choice of initial guess [9, 21]. For a practical mechanical control system, possibly the best strategy would be to utilise the strength of both gradient-based and Newton-based solvers [33]. A vague initial guess might be extremely far from the optimal solution. Therefore, we propose two hybrid solution strategies which in a first step make use of a staggered FBSM gradient-based solver with a suitable Barzilai-Borwein accelerator[3, 13, 41] to reach the vicinity of the optimal solution or improve the quality of the initial guess, and then, in a second step, apply a Newton-based solver to achieve high precision optimal trajectories.

We first study the performance of the individual monolithic and staggered FBSM solvers based on Newton's method, and then the possible advantages of the hybrid solution strategies with an increase in the size of the NLP. For a fair comparison, the same initial guess is provided to all solvers and their performance is evaluated based on the total computational time taken and number of iterations. To this end, we choose a set of representative two- and three-dimensional examples with and without holonomic mechanical constraints that allow us to evaluate the performance of the proposed alternative solvers with respect to their robustness and accuracy.

The article is structured as follows: Section 2 introduces the natural description of constrained mechanical systems in terms of index-3 DAEs. In Section 3, we formulate optimal control problems based on ODEs and DAEs as state equations, together with the corresponding necessary conditions of optimality and conservation laws. Section 4 presents the symplectic integration method applied throughout this work. The corresponding discrete conditions of optimality give rise to a NLP whose solution is addressed in Section 5. Section 6, provides numerical examples to study the numerical performance of the alternative solution strategies proposed. Finally, conclusions are drawn in Section 7.

2 Constrained mechanical system: Index-3 DAEs

We consider a mechanical system evolving over a n dimensional configuration manifold $\mathcal{Q}$ with configuration coordinates $\boldsymbol{q} := \{\boldsymbol{q}^1, \boldsymbol{q}^2, \cdots, \boldsymbol{q}^n\} \in \mathcal{Q}$. At time $t \in \mathcal{I} := [0, T] \subset \mathbb{R}_0^+$, position $\boldsymbol{q}$ and velocity $\dot{\boldsymbol{q}} := \frac{d\boldsymbol{q}}{dt} \in \mathcal{T}_q\mathcal{Q}$ form the state-space $(\boldsymbol{q}, \dot{\boldsymbol{q}}) \in \mathcal{T}\mathcal{Q}$, whereas the configuration coordinates $\boldsymbol{q}$ together with the momentum vector $\boldsymbol{p} = \mathbf{M}\dot{\boldsymbol{q}} \in \mathcal{T}_q^*\mathcal{Q}$ form the canonical phase space $(\boldsymbol{q}, \boldsymbol{p}) \in \mathcal{T}^*\mathcal{Q}$. Here, mass matrix $\mathbf{M}$ is assumed to be configuration invariant and nondegenerate [1, 24, 30]. Furthermore, in the presence of geometric constraints (scleronomic) on $\mathcal{Q}$ we impose holonomic

constraints $\boldsymbol{\Phi} : \mathcal{Q} \to \mathbb{R}^d$ (with $d < n$) by introducing Lagrange multipliers $\boldsymbol{\lambda} \in (\mathbb{R}^d)^* \cong \mathbb{R}^d$ and define a $(n-d)$ dimensional constraint submanifold $\mathcal{M} := \{\boldsymbol{q} \in \mathcal{Q} : \boldsymbol{\Phi}(\boldsymbol{q}) = \boldsymbol{0}\} \subset \mathcal{Q}$. Then, the system dynamics evolves over phase-space $\mathcal{P} = \mathcal{T}^*\mathcal{M} = \{(\boldsymbol{q}, \boldsymbol{p}) \in \mathcal{T}^*\mathcal{Q} : \boldsymbol{\Phi}(\boldsymbol{q}) = \boldsymbol{0}, \nabla_{\boldsymbol{q}}\boldsymbol{\Phi} \cdot \mathbf{M}^{-1}\boldsymbol{p} = \boldsymbol{0}\}$ which is a $2(n-d)$ dimensional submanifold [6, 27]. For simplicity, we assume a controlling force $\boldsymbol{u} := \{u_1, \cdots, u_m\} \in \mathcal{U} \subset \mathbb{R}^m$, with $\mathcal{U}$ a space of admissible control. For a constrained mechanical system with the notion of augmented Hamiltonian $\mathcal{E} : \mathcal{T}^*\mathcal{Q} \times (\mathbb{R}^d)^* \to \mathbb{R}$, the equations of motion constitute index-3 differential-algebraic equations (DAEs). For the numerical treatment, governing equations expressed in first-order form read [6]

$$\begin{aligned} \dot{\boldsymbol{q}} &= \nabla_{\boldsymbol{p}}\mathcal{E}(\boldsymbol{q}, \boldsymbol{p}, \boldsymbol{\lambda}) \\ \dot{\boldsymbol{p}} &= -\nabla_{\boldsymbol{q}}\mathcal{E}(\boldsymbol{q}, \boldsymbol{p}, \boldsymbol{\lambda}) + \boldsymbol{u} \\ \boldsymbol{0} &= \nabla_{\boldsymbol{\lambda}}\mathcal{E}(\boldsymbol{q}, \boldsymbol{p}, \boldsymbol{\lambda}) \end{aligned} \tag{1}$$

where $\mathcal{E}(\boldsymbol{q}, \boldsymbol{p}, \boldsymbol{\lambda}) := \frac{1}{2}\boldsymbol{p}^T\mathbf{M}^{-1}\boldsymbol{p} + \mathcal{V}(\boldsymbol{q}) + \boldsymbol{\Phi}(\boldsymbol{q})^T\boldsymbol{\lambda}$, $\mathcal{V} : \mathcal{Q} \to \mathbb{R}$ is the potential energy and $\nabla_{(\bullet)}$ is the partial derivative w.r.t $(\bullet)$. In the absence of external force, $\boldsymbol{u} = \boldsymbol{0}$, the augmented Hamiltonian is an invariant of the motion i.e., $\dot{\mathcal{E}} = 0$. Introducing phase-space coordinates $\boldsymbol{y} := (\boldsymbol{y}_q, \boldsymbol{y}_p) \in \mathcal{T}^*\mathcal{Q}$, corresponding to the original vectors $(\boldsymbol{q}, \boldsymbol{p})$, we retrieve the following state-space representation of the underlying constrained mechanical control system

$$\begin{aligned} \dot{\boldsymbol{y}} &= \boldsymbol{f}(\boldsymbol{y}, \boldsymbol{\lambda}, \boldsymbol{u}) \\ \boldsymbol{0} &= \boldsymbol{\Phi}_q(\boldsymbol{y}) \end{aligned} \tag{2}$$

where $\boldsymbol{\Phi}_q(\boldsymbol{y}) = \boldsymbol{\Phi} \circ \pi_{\mathcal{Q}}$ indicates that the constraints only depend on $\boldsymbol{y}_q = \boldsymbol{q}$, and $\pi_{\mathcal{Q}} = \mathcal{T}^*\mathcal{Q} \to \mathcal{Q}$ denotes the projection on the configuration coordinates. We restrict this apparent general form of the force field to the following form

$$\boldsymbol{f}(\boldsymbol{y}, \boldsymbol{\lambda}, \boldsymbol{u}) := \begin{bmatrix} \boldsymbol{f}^q(\boldsymbol{p}) \\ \boldsymbol{f}^p(\boldsymbol{q}, \boldsymbol{u}, \boldsymbol{\lambda}) \end{bmatrix} = \begin{bmatrix} \mathbf{M}^{-1}\boldsymbol{p} \\ \boldsymbol{u} + \boldsymbol{f}^{int}(\boldsymbol{q}) + \boldsymbol{f}^c(\boldsymbol{q}, \boldsymbol{\lambda}) \end{bmatrix} \tag{3}$$

with $\boldsymbol{f}^{int}(\boldsymbol{q}) := -\nabla_{\boldsymbol{q}}\mathcal{V}(\boldsymbol{q})$ the internal force due to conservative forces, and $\boldsymbol{f}^c(\boldsymbol{q}, \boldsymbol{\lambda}) := -\nabla_{\boldsymbol{q}}\boldsymbol{\Phi}_q(\boldsymbol{q})^T\boldsymbol{\lambda}$, the constraint force that prevents the system from leaving the constraint manifold.

Remark 1. The above system in Eq (2) must be complemented with the appropriate initial or boundary conditions consistent with the holonomic constraints. The above index-3 DAE representation in redundant coordinates provides an elegant way to circumvent the singularities and convoluted index reduction procedure associated with the minimal coordinate representation of a constrained mechanical system expressed as an ordinary differential equation (ODE). Note that in the absence of holonomic constraints, our mechanical control system reduces to the standard state space ODE governed by $\dot{\boldsymbol{y}} = \boldsymbol{f}(\boldsymbol{y}, \boldsymbol{u})$ and the dynamics evolves over cotangent bundle $\mathcal{T}^*\mathcal{Q}$.

3 Optimal control problem (OCP)

In this section, we discuss the optimal control of mechanical systems expressed in redundant coordinates (DAEs). We deduce first the necessary conditions of optimality, conservation laws and inherent symplectic structure of the solution.

3.1 Optimal control with state equations in DAE form (OCP-DAE)

In this subsection, we shall derive the first-order necessary conditions for a mechanical optimal control system whose configuration and control space are expressed in redundant coordinates $\boldsymbol{y}(t)$, from its initial state $\boldsymbol{y}(0) = \overline{\boldsymbol{y}}_0$ to a final state $\boldsymbol{y}(T) = \boldsymbol{y}_d$, and subjected to the holonomic constraint $\boldsymbol{\Phi}_q(\boldsymbol{y}) = \boldsymbol{0}$. Let us consider the optimal control problem subjected to semi-explicit index-3 DAEs (see Eq (2)) where we aim to deduce the optimal evolution of the force vector $\boldsymbol{u} \in \mathcal{U}$ that minimises a given functional $\mathcal{J} : \mathcal{P} \times \mathcal{U} \to \mathbb{R}$ in a given amount of time $T \in \mathcal{I}$. To achieve this objective, we state the following two minimisation problems [9, 15]

$$\begin{aligned} &\min_{\boldsymbol{y}, \boldsymbol{u}} \int_0^T \mathcal{L}(\boldsymbol{y}, \boldsymbol{u}) dt \\ &\text{s.t., } \boldsymbol{f}(\boldsymbol{y}, \boldsymbol{u}) - \dot{\boldsymbol{y}} = \boldsymbol{0} \\ &\qquad \boldsymbol{\Phi}_q(\boldsymbol{y}) = \boldsymbol{0} \\ &\qquad \boldsymbol{g}_T(\boldsymbol{y}(T)) = \boldsymbol{0} \\ &\qquad \boldsymbol{g}_0(\boldsymbol{y}(0)) = \boldsymbol{0} \end{aligned} \tag{4}$$

$$
\begin{aligned}
&\min_{\boldsymbol{y},\boldsymbol{u}} \int_0^T \mathcal{L}(\boldsymbol{y},\boldsymbol{u})dt + \psi(\boldsymbol{y}(T)) \\
&\text{s.t., } \boldsymbol{f}(\boldsymbol{y},\boldsymbol{u}) - \dot{\boldsymbol{y}} = \boldsymbol{0} \\
&\quad \boldsymbol{\Phi}_q(\boldsymbol{y}) = \boldsymbol{0} \\
&\quad \boldsymbol{g}_0(\boldsymbol{y}(0)) = \boldsymbol{0}
\end{aligned} \tag{5}
$$

where, $\boldsymbol{g}_0(\boldsymbol{y}(0)) := \boldsymbol{y}(0) - \overline{\boldsymbol{y}}_0$ is the initial state constraint, and $\boldsymbol{g}_T(\boldsymbol{y}(T)) := \boldsymbol{y}(T) - \boldsymbol{y}_d$ is the final state constraint, which imposes the final state $\boldsymbol{y}_d$ at time $t = T$. Problem (4) is known as Lagrange OCP, while problem (5) is called Bolza OCP (or penalty type OCP). Then, we combine both Lagrange and Bolza forms into the following Bolza-type minimisation problem

$$
\begin{aligned}
&\min_{\boldsymbol{y},\boldsymbol{u}} \mathcal{J}(\boldsymbol{y},\boldsymbol{u}) \\
&\text{s.t., } \boldsymbol{f}(\boldsymbol{y},\boldsymbol{\lambda},\boldsymbol{u}) - \dot{\boldsymbol{y}} = \boldsymbol{0} \\
&\quad \boldsymbol{\Phi}_q(\boldsymbol{y}) = \boldsymbol{0} \\
&\quad \gamma \boldsymbol{g}_T(\boldsymbol{y}(T)) = \boldsymbol{0} \\
&\quad \boldsymbol{g}_0(\boldsymbol{y}(0)) = \boldsymbol{0}
\end{aligned} \tag{6}
$$

where the objective functional $\mathcal{J} : \mathcal{P} \times \mathcal{U} \to \mathbb{R}$ is given by

$$
\mathcal{J}(\boldsymbol{y},\boldsymbol{u}) = \int_0^T \mathcal{L}(\boldsymbol{y},\boldsymbol{u})dt + \beta_T \psi(\boldsymbol{y}(T)). \tag{7}
$$

and $\gamma \in \{1, 0\}$ and $\beta_T \in \mathbb{R}_0^+$. For the choices $(\gamma, \beta_T) = (1, 0)$ and $(\gamma, \beta_T) = (0, \gg 1)$, we obtain standard Lagrange and Bolza type OCP, respectively. Here, we consider the quadratic form of the tracking type running ($\mathcal{L} : \mathcal{P} \times \mathcal{U} \to \mathbb{R}$) and terminal costs ($\psi : \mathcal{P} \to \mathbb{R}$), defined as

$$
\mathcal{L}(\boldsymbol{y}(t),\boldsymbol{u}(t)) = \frac{\beta}{2}(\boldsymbol{y}(t) - \boldsymbol{y}_d(t))^T(\boldsymbol{y}(t) - \boldsymbol{y}_d(t)) + \frac{\alpha}{2}\boldsymbol{u}(t)^T\boldsymbol{u}(t), \tag{8}
$$

$$
\psi(\boldsymbol{y}(T)) = \frac{1}{2}(\boldsymbol{y}(T) - \boldsymbol{y}_d(T))^T(\boldsymbol{y}(T) - \boldsymbol{y}_d(T)), \tag{9}
$$

where $\alpha, \beta \in \mathbb{R}_0^+$, and the time horizon $T \in \mathcal{I}$ is known. We assume that the initial and final state constraints, $\boldsymbol{g}_0(\boldsymbol{y}(0)) = \boldsymbol{0}$ and $\boldsymbol{g}_T(\boldsymbol{y}(T)) = \boldsymbol{0}$, fulfil the geometric constraint on the position level as well as on the momentum level. We point out that the running and terminal functions, respectively $\mathcal{L}(\boldsymbol{y},\boldsymbol{u})$ and $\psi(\boldsymbol{y})$ in (8)-(9), are smooth quadratic functions, and that we assume that our admissible set $\mathcal{U}$ is convex and unbounded. This will motivate our numerical solution procedure in Section 5.

Next, we introduce adjoint variables $\boldsymbol{\mu}(t) \in \mathcal{T}^*\mathcal{P}$, $\boldsymbol{\zeta}(t) \in (\mathbb{R}^d)^*$, $\boldsymbol{\nu} \in \mathbb{R}^{\dim(\boldsymbol{g}_0)}$ and $\boldsymbol{\eta} \in \mathbb{R}^{\dim(\boldsymbol{g}_T)}$ and adjoin the constraint with the cost functional $\mathcal{J}$ and define the augmented Lagrangian functional $\mathcal{S}$

$$
\begin{aligned}
\mathcal{S}(\boldsymbol{y},\boldsymbol{\lambda},\boldsymbol{u};\boldsymbol{\mu},\boldsymbol{\zeta},\boldsymbol{\eta},\boldsymbol{\nu}) := \int_0^T \Big(\mathcal{L}(\boldsymbol{y},\boldsymbol{u}) + \boldsymbol{\mu}^{\mathsf{T}}(\boldsymbol{f}(\boldsymbol{y},\boldsymbol{\lambda},\boldsymbol{u}) - \dot{\boldsymbol{y}}) + \boldsymbol{\zeta}^{\mathsf{T}}\boldsymbol{\Phi}_q(\boldsymbol{y})\Big)\, dt + \boldsymbol{\nu}^{\mathsf{T}}\boldsymbol{g}_0(\boldsymbol{y}(0)) \\
+\gamma\boldsymbol{\eta}^{\mathsf{T}}\boldsymbol{g}_T(\boldsymbol{y}(T)) + \beta_T\psi(\boldsymbol{y}(T)).
\end{aligned} \tag{10}
$$

With the notion of control Hamiltonian $\mathcal{H}$ associated with OCP-DAE in Eq (6)

$$
\mathcal{H}(\boldsymbol{y},\boldsymbol{\lambda},\boldsymbol{u};\boldsymbol{\mu},\boldsymbol{\zeta}) = \mathcal{L}(\boldsymbol{y},\boldsymbol{u}) + \boldsymbol{\mu}^{\mathsf{T}}\boldsymbol{f}(\boldsymbol{y},\boldsymbol{\lambda},\boldsymbol{u}) + \boldsymbol{\zeta}^{\mathsf{T}}\boldsymbol{\Phi}_q(\boldsymbol{y}) \tag{11}
$$

the first-order necessary conditions of optimality furnish a system of DAEs given by [13]

$$
\begin{aligned}
\dot{\boldsymbol{y}} &= \nabla_{\boldsymbol{\mu}}\mathcal{H} \\
\boldsymbol{0} &= \nabla_{\boldsymbol{\zeta}}\mathcal{H} \\
\dot{\boldsymbol{\mu}} &= -\nabla_{\boldsymbol{y}}\mathcal{H} \\
\boldsymbol{0} &= \nabla_{\boldsymbol{\lambda}}\mathcal{H} \\
\boldsymbol{0} &= \nabla_{\boldsymbol{u}}\mathcal{H}
\end{aligned} \tag{12a}
$$

with the BCs,

$$
\begin{aligned}
&\boldsymbol{g}_0(\boldsymbol{y}(0)) = \boldsymbol{0},\ \boldsymbol{\mu}(0) = -\nabla_{\boldsymbol{y}(0)}\boldsymbol{g}_0(\boldsymbol{y}(0))^{\mathsf{T}}\boldsymbol{\nu}, \\
&\gamma\boldsymbol{g}_T(\boldsymbol{y}(T)) = \boldsymbol{0},\ \boldsymbol{\mu}(T) = \nabla_{\boldsymbol{y}(T)}\left(\beta_T\psi(\boldsymbol{y}(T)) + \gamma\boldsymbol{g}_T(\boldsymbol{y}(T))^{\mathsf{T}}\boldsymbol{\eta}\right).
\end{aligned} \tag{12b}
$$

If we collect the differential coordinates into $\boldsymbol{z} = (\boldsymbol{y}, \boldsymbol{\mu})$ and the algebraic coordinates into $\boldsymbol{s} = (\boldsymbol{\lambda}, \boldsymbol{\zeta}, \boldsymbol{u})$, the above stationarity conditions can be written in the following compact form which reveals the symplectic structure of the state-adjoint system,

$$\begin{aligned} \dot{\boldsymbol{z}} &= \mathbb{J}\nabla_{\boldsymbol{z}}\mathcal{H}(\boldsymbol{z}, \boldsymbol{s}) \\ \mathbf{0} &= \nabla_{\boldsymbol{s}}\mathcal{H}(\boldsymbol{z}, \boldsymbol{s}). \end{aligned} \tag{13}$$

where $\mathbb{J} := \begin{bmatrix} \mathbf{0} & \mathbf{I} \\ -\mathbf{I} & \mathbf{0} \end{bmatrix}$ is the canonical symplectic matrix ($\mathbb{J}^{-1} = \mathbb{J}^{\mathsf{T}}$), with $\mathbf{0}$ and $\mathbf{I}$ denoting $2n \times 2n$ null and identity matrices, respectively. Note that the Hamiltonian boundary value problem (HBVP) (12a) reduces to the standard HBVP in OCPs with $\boldsymbol{s} = \boldsymbol{u}$ if the holonomic constraints are removed, in which case we deal with a OCP-ODE instead of OCP-DAE. Also, we note that due to the presence of the mechanical constraints, which may introduce singularities and yield degenerated solutions, we shall talk of a presymplectic structure rather than symplectic [17, 22].

From a geometric point of view, the state-adjoint space of the control Hamiltonian system forms an even-dimensional symplectic manifold with the symplectic two-form $\Omega := d\boldsymbol{y} \wedge d\boldsymbol{\mu}$, where $\wedge$ denotes the exterior product. With coordinates $\boldsymbol{z} := (\boldsymbol{y}, \boldsymbol{\mu})$, the optimality conditions retrieve their canonical form which highlights that the flow of the state-adjoint system is symplectic (and thus preserves the symplectic structure) or divergence-free i.e. $\nabla_{\boldsymbol{z}} \cdot \dot{\boldsymbol{z}} = 0$ (Liouville's theorem) [23]. While the simplecticity of the form in the first block equation in (13) is clear [1, 23], the presence of the constraint $\nabla_s\mathcal{H}(\boldsymbol{z}, \boldsymbol{s}) = \mathbf{0}$ and the dependence of $\boldsymbol{s}$ on the state and co-state variable in $\boldsymbol{z}$ makes the symplecticity less evident. For this reason, we explicitly show in Appendix A that if the system can be projected on a set of minimal coordinates $\boldsymbol{y}$, or in the absence of holonomic constraints (i.e. $\boldsymbol{s} = \boldsymbol{u}$), the preservation of the area on the phase space $(\boldsymbol{y}, \boldsymbol{\mu})$ is retained for an optimal $\boldsymbol{s}$ and a system with the form in (13), provided some regularity conditions on $\mathcal{H}$ are satisfied.

Remark 2. The Lagrange OCP with choice $(\gamma, \beta_T) = (1, 0)$ prescribes the final state $\boldsymbol{y}(T) = \boldsymbol{y}_d(T)$ and results in unknown adjoints at the final time ($\boldsymbol{\mu}(T)$). In other words, enforcing the end constraint $\boldsymbol{g}_T(\boldsymbol{y}(T)) = \mathbf{0}$ with multiplier $\boldsymbol{\eta}$ furnishes $\boldsymbol{\mu}(T) = \boldsymbol{\eta}$, which is not an explicit function of $\boldsymbol{y}(T)$. Alternatively, the combination $(\gamma, \beta_T) = (0, \gg 1)$ results in transversality conditions for the adjoints as a sole function of the state, i.e. $\boldsymbol{\mu}(T) = \beta_T \nabla_{\boldsymbol{y}(T)}\psi(\boldsymbol{y}(T))$, and constitutes a penalty formulation of the OCP. Moreover, combination $(\alpha = 1, \beta = \beta_T = 0)$ forms the minimal effort Lagrange OCP, whereas the combination $(\beta = 0, \beta_T \approx 1, \alpha/\beta_T \leq 10^{-3})$ gives rise to the penalty minimal effort OCP. The adjoints of minimal effort penalty and Lagrange OCP ($\boldsymbol{\mu}^*$ and $\boldsymbol{\mu}$, respectively) are related by the relation $\boldsymbol{\mu}^* = \alpha\boldsymbol{\mu}$. This relation is deduced by equating the control Hamiltonian of both problems i.e., $\mathcal{H}(\boldsymbol{y}, \boldsymbol{u}, \boldsymbol{\mu}^*)/\alpha = \mathcal{H}(\boldsymbol{y}, \boldsymbol{u}, \boldsymbol{\mu})_{(\alpha=1)}$ with $\beta_T = 1$.

Remark 3. We point out that the presence holonomic constraints $\boldsymbol{\Phi}(\boldsymbol{q}) = \mathbf{0}$ lead to redundancies at the boundary, and one must be careful while formulating boundary conditions for OCP-DAE with $\gamma = 1, \beta_T = 0$. A null space projection $\mathbf{P} : \mathcal{TQ} \to \mathcal{TM}$ gives the relation between admissible variations in redundant and minimal configuration coordinates such that $\delta\boldsymbol{q} = \mathbf{P}(\boldsymbol{q})\delta\boldsymbol{q}^{red}$, where $\mathbf{P}(\boldsymbol{q})$ is a null-space matrix which is the orthogonal complement of the constraint Jacobian ($\nabla_{\boldsymbol{q}}\boldsymbol{\Phi}(\boldsymbol{q}) \cdot \mathbf{P}(\boldsymbol{q}) = \mathbf{0}$) [26, 27, 41]. In our examples, by setting $\boldsymbol{y}_d = (\boldsymbol{q}_d, \boldsymbol{p}_d)$ the prescribed end conditions for the states, our final conditions read

$$\boldsymbol{g}_T(\boldsymbol{y}) = \left\{ \begin{array}{c} \mathbf{P}(\boldsymbol{q}_d)^{\mathsf{T}}(\boldsymbol{q} - \boldsymbol{q}_d) \\ \boldsymbol{p} - \boldsymbol{p}_d \end{array} \right\} = \mathbf{D}(\boldsymbol{y} - \boldsymbol{y}_d) \tag{14}$$

with

$$\mathbf{D} = \left[\begin{array}{cc} \mathbf{P}(\boldsymbol{q}_d)^T & \mathbf{0} \\ \mathbf{0} & \mathbf{I} \end{array} \right].$$

We also note that similar null-space projection may be applied on variable $\boldsymbol{\mu}$, which is also constrained through the algebraic equation $\mathbf{0} = \nabla_{\lambda}\mathcal{H}$.

Alternatively, a more convenient way to get rid of these redundancies is to regularise the problem by adding sufficiently small weight $\beta_T \approx 10^{-3}$ of the terminal cost $\psi(\boldsymbol{y}(T))$ in the cost functional. For minimal effort optimal control of complex mechanical systems ill-conditioning problems associated with the prescribed state at the final time can be efficiently handled with penalty formulation of OCP-DAE ($\gamma = 0, \beta_T = 1$). Our numerical experiments show that for sufficiently small $\alpha/\beta_T \approx 10^{-3}$ the penalty approach yields satisfactory results and optimal trajectories are in close agreement with the Lagrange form of OCP-DAE ($\gamma = 1, \beta_T = 0$). More details on this can be found in numerical examples 6.1 and 6.2.

3.2 Symmetries and conservation laws of the optimal control problem

In the previous section, we have seen that the optimal control problem satisfies Hamilton equations (see Eq (13)). Noether's theorem ensures the existence of conserved quantities corresponding to

admissible transformations which leave the control Hamiltonian invariant [16, 44]. In other words, if the control Hamiltonian is independent of coordinate y_i, then we say y_i is cyclic ($\frac{\partial \mathcal{H}}{\partial y_i} = 0$) and there is some quantity which is a first integral of the motion. In the context of OCP-DAE, we now present the conservation laws corresponding to time translation and rotational symmetries [4, 40]. Similarly to the partition of the differential state variables, $\boldsymbol{y} = (\boldsymbol{q}, \boldsymbol{p}) = (\boldsymbol{q}^1, \cdots, \boldsymbol{q}^n, \boldsymbol{p}^1, \cdots, \boldsymbol{p}^n)$, we partition the differential adjoint variables, $\boldsymbol{\mu} = (\boldsymbol{\mu}^q, \boldsymbol{\mu}^p) = ((\boldsymbol{\mu}^q)^1, \cdots, (\boldsymbol{\mu}^q)^n, (\boldsymbol{\mu}^p)^1, \cdots, (\boldsymbol{\mu}^p)^n)$.

Proposition 1. *For an autonomous optimal control problem, the control Hamiltonian is a first integral of the motion, i.e.,* $\dot{\mathcal{H}} = 0$.

Proof. The total time derivative of control Hamiltonian $\mathcal{H}(\boldsymbol{z}, \boldsymbol{s}, t)$ yields

$$\frac{d\mathcal{H}}{dt} = \nabla_{\boldsymbol{z}}\mathcal{H} \cdot \dot{\boldsymbol{z}} + \nabla_{\boldsymbol{s}}\mathcal{H} \cdot \dot{\boldsymbol{s}} + \partial_t \mathcal{H}$$

For an autonomous system, $\partial_t \mathcal{H} = 0$. Using the optimality conditions (see Eq (13)), we get $\dot{\mathcal{H}} = 0$. □

Proposition 2. *If the control Hamiltonian is invariant under superimposed rigid rotations about an axis whose direction is given by an unit vector* $\boldsymbol{n}$*, then the quantity* $\boldsymbol{\xi} \cdot \boldsymbol{n}$ *is a first-integral of the motion, where*

$$\boldsymbol{\xi} := \boldsymbol{y} \star \boldsymbol{\mu} = \sum_{i=1}^{n} \boldsymbol{q}^i \times (\boldsymbol{\mu}^q)^i + \boldsymbol{p}^i \times (\boldsymbol{\mu}^p)^i \tag{15}$$

In what follows we call $\boldsymbol{\xi}$ *the control angular momentum. Unfortunately, up to now there is no physical interpretation for the corresponding symmetry available in the literature.*

Proof. The rate of change of control Hamiltonian $\mathcal{H}(\boldsymbol{z}, \boldsymbol{s})$ w.r.t. rigid rotations $\theta \in \mathbb{R}$ about constant axis $\boldsymbol{n}$ is given by

$$\frac{d\mathcal{H}}{d\theta} = \nabla_{\boldsymbol{z}}\mathcal{H} \cdot \frac{d\boldsymbol{z}}{d\theta} + \nabla_{\boldsymbol{s}}\mathcal{H} \cdot \frac{d\boldsymbol{s}}{d\theta} + \partial_\theta \mathcal{H}$$

Using the optimality conditions (see Eq (13)) and assuming $\mathcal{H}$ is not an explicit function of θ, i.e. $\partial_\theta \mathcal{H} = 0$, we obtain (recall $\mathbb{J}^{-1} = \mathbb{J}^{\mathsf{T}}$)

$$\frac{d\mathcal{H}}{d\theta} = \dot{\boldsymbol{z}} \cdot \mathbb{J}\frac{d\boldsymbol{z}}{d\theta} = \dot{\boldsymbol{q}} \cdot \frac{d\boldsymbol{\mu}^q}{d\theta} - \dot{\boldsymbol{\mu}}^q \cdot \frac{d\boldsymbol{q}}{d\theta} + \dot{\boldsymbol{p}} \cdot \frac{d\boldsymbol{\mu}^p}{d\theta} - \dot{\boldsymbol{\mu}}^p \cdot \frac{d\boldsymbol{p}}{d\theta} \tag{16}$$

Since the phase space (cotangent space) of the optimal control problem at a point $(\boldsymbol{y}, \boldsymbol{\mu})$ is a real vector space of dimension $12n$, the superimposed rotation on the mechanical system can be viewed as the rotation of 3-dimensional $4n$ state-adjoint vectors in $\mathbb{R}^3$. The differential change of a vector $\boldsymbol{q}^i \in \mathbb{R}^3$ due to the superimposed rigid rotation $d\theta$ about axis $\boldsymbol{n} \in \mathbb{R}^3$ is given by $d\boldsymbol{q}^i = d\theta\left(\boldsymbol{n} \times \boldsymbol{q}^i\right)$, i.e. $d\boldsymbol{q}^i/d\theta = \boldsymbol{n} \times \boldsymbol{q}^i$, and equally for vectors $\boldsymbol{p}^i, (\boldsymbol{\mu}^q)^i$ and $(\boldsymbol{\mu}^p)^i$. Using these expressions in equation (16) along with the properties of the vector triple product, we have

$$\frac{d\mathcal{H}}{d\theta} = -\boldsymbol{n} \cdot \frac{d}{dt}\left(\sum_{i=1}^{n} \boldsymbol{q}^i \times (\boldsymbol{\mu}^q)^i + \boldsymbol{p}^i \times (\boldsymbol{\mu}^p)^i\right) =: -\boldsymbol{n} \cdot \frac{d}{dt}(\boldsymbol{y} \star \boldsymbol{\mu})$$

If the control Hamiltonian has the symmetry stipulated above, then $\frac{d\mathcal{H}}{d\theta} = 0$ and we get

$$\boldsymbol{n} \cdot \frac{d}{dt}(\boldsymbol{y} \star \boldsymbol{\mu}) = 0$$

Hence, the component of the control angular momentum $\boldsymbol{\xi} := \boldsymbol{y} \star \boldsymbol{\mu}$ along $\boldsymbol{n}$ is an integral/invariant of the motion. That is,

$$\dot{\boldsymbol{\xi}} \cdot \boldsymbol{n} = 0$$

□

In case the mechanical control system has rotational invariance about arbitrary axis $\boldsymbol{n} \in \mathbb{R}^3$, then all three components of the control angular momentum are preserved.

For complex constrained mechanical systems, identification of time translation symmetry of the control Hamiltonian is straightforward and often fulfilled. However, the identification of rotational symmetry is not always a trivial task. Considering this, we provide certain conditions to evaluate the rotational invariance of the control Hamiltonian in a much more convenient manner.

Proposition 3. *Consider a mechanical control system under a superimposed rigid rotation* $(\boldsymbol{q}, \boldsymbol{p}, \boldsymbol{\mu}^q, \boldsymbol{\mu}^p, \boldsymbol{u}) \to (\overline{\boldsymbol{q}}, \overline{\boldsymbol{p}}, \overline{\boldsymbol{\mu}}^q, \overline{\boldsymbol{\mu}}^p, \overline{\boldsymbol{u}})$ *about* $\boldsymbol{n} \in \mathbb{R}^3$ *such that* $\overline{\boldsymbol{q}}^i = \mathbf{R}\boldsymbol{q}^i, \overline{\boldsymbol{p}}^i = \mathbf{R}\boldsymbol{p}^i, (\overline{\boldsymbol{\mu}}^q)^i = \mathbf{R}(\boldsymbol{\mu}^q)^i, (\overline{\boldsymbol{\mu}}^p)^i = \mathbf{R}(\boldsymbol{\mu}^p)^i, \overline{\boldsymbol{u}}^i = \mathbf{R}\boldsymbol{u}^i$ *where* $i = 1, \cdots, n$ *and* $\mathbf{R} \in \mathbf{SO}(3)$ *is the rotation matrix about* $\boldsymbol{n}$*. If the following conditions are satisfied:*

1. $\mathcal{L}(\overline{\boldsymbol{q}}, \overline{\boldsymbol{p}}, \overline{\boldsymbol{u}}) = \mathcal{L}(\boldsymbol{q}, \boldsymbol{p}, \boldsymbol{u})$
2. $\boldsymbol{\Phi}(\overline{\boldsymbol{q}}) = \boldsymbol{\Phi}(\boldsymbol{q})$
3. $\boldsymbol{f}^q(\overline{\boldsymbol{p}})^i = \mathbf{R}\boldsymbol{f}^q(\boldsymbol{p})^i$
4. $\boldsymbol{f}^p(\overline{\boldsymbol{q}}, \overline{\boldsymbol{p}}, \overline{\boldsymbol{u}}, \boldsymbol{\lambda})^i = \mathbf{R}\boldsymbol{f}^p(\boldsymbol{q}, \boldsymbol{p}, \boldsymbol{u}, \boldsymbol{\lambda})^i$

then the component of control angular momentum $\boldsymbol{\xi}$ along $\boldsymbol{n}$ is an invariant of motion.

Proof. Control Hamiltonian under superimposed rigid rotation reads (see Eq (11))

$$\mathcal{H}(\overline{\boldsymbol{q}}, \overline{\boldsymbol{p}}, \boldsymbol{\lambda}, \overline{\boldsymbol{u}}; \overline{\boldsymbol{\mu}}^q, \overline{\boldsymbol{\mu}}^p, \boldsymbol{\zeta}) = \mathcal{L}(\overline{\boldsymbol{q}}, \overline{\boldsymbol{p}}, \overline{\boldsymbol{u}}) + \overline{\boldsymbol{\mu}}^q \cdot \boldsymbol{f}^q(\overline{\boldsymbol{p}}) + \overline{\boldsymbol{\mu}}^p \cdot \boldsymbol{f}^p(\overline{\boldsymbol{q}}, \overline{\boldsymbol{p}}, \boldsymbol{\lambda}) + \boldsymbol{\zeta} \cdot \boldsymbol{\Phi}(\overline{\boldsymbol{q}})$$

Using above four conditions and orthogonality of rotation matrices ($\mathbf{R}^T\mathbf{R} = \mathbf{I}$), we obtain (sum over $i = 1, \cdots, n$)

$$\begin{aligned}
\mathcal{H}(\overline{\boldsymbol{q}}, \overline{\boldsymbol{p}}, \boldsymbol{\lambda}, \overline{\boldsymbol{u}}; \overline{\boldsymbol{\mu}}^q, \overline{\boldsymbol{\mu}}^p, \boldsymbol{\zeta}) &= \mathcal{L}(\boldsymbol{q}, \boldsymbol{p}, \boldsymbol{u}) + (\overline{\boldsymbol{\mu}}^q)^i \cdot \mathbf{R}\boldsymbol{f}^q(\boldsymbol{p})^i + (\overline{\boldsymbol{\mu}}^p)^i \cdot \mathbf{R}\boldsymbol{f}^p(\boldsymbol{q}, \boldsymbol{p}, \boldsymbol{\lambda})^i + \boldsymbol{\zeta} \cdot \boldsymbol{\Phi}(\boldsymbol{q}) \\
&= \mathcal{L}(\boldsymbol{q}, \boldsymbol{p}, \boldsymbol{u}) + (\boldsymbol{\mu}^q)^i \cdot \boldsymbol{f}^q(\boldsymbol{p})^i + (\boldsymbol{\mu}^p)^i \cdot \boldsymbol{f}^p(\boldsymbol{q}, \boldsymbol{p}, \boldsymbol{\lambda})^i + \boldsymbol{\zeta} \cdot \boldsymbol{\Phi}(\boldsymbol{q}) \\
&= \mathcal{H}(\boldsymbol{q}, \boldsymbol{p}, \boldsymbol{\lambda}, \boldsymbol{u}; \boldsymbol{\mu}^q, \boldsymbol{\mu}^p, \boldsymbol{\zeta}).
\end{aligned}$$

Since the control Hamiltonian is invariant under superimposed rigid rotation, it follows from Proposition 2 that the component of control angular momentum $\boldsymbol{\xi}$ along $\boldsymbol{n}$ is an integral of motion. □

4 Temporal discretisation

In this section, we construct a numerical integrator which preserves the symplectic structure of the solution while preserving the constraints. An additional advantage of symplectic integrators is that they automatically preserve the momentum maps corresponding to the symmetries of the mechanical control system [4]. We are mainly interested in symplectic discretisation, which yields the same nonlinear programming problem (NLP) irrespective of indirect and direct approaches to OCP. We have opted to discretisation schemes that preserve the symplectic structure of the OCP in (12a), but that spoil the symplectic structure of the underlying mechanical system in (1). The latter is in fact only symplectic when no external loads exist, which is not the case for control problems.

We begin with the partition of time domain $\mathcal{I} := [0, T]$ into N uniform non-overlapping segments with constant step size $\Delta t > 0$. Next, we approximate the exact flow (see Eq (12a)) at discrete time points with the Symplectic Euler time-integration scheme (hereby referred to as SE1 scheme) as depicted in the Box 1.

$$\begin{aligned}
\boldsymbol{y}_n - \boldsymbol{y}_{n-1} &= \Delta t \nabla_{\boldsymbol{\mu}} \mathcal{H}(\boldsymbol{y}_n, \boldsymbol{\lambda}_n, \boldsymbol{u}_{n-1}, \boldsymbol{\mu}_{n-1}, \boldsymbol{\zeta}_{n-1}), \\
\boldsymbol{\mu}_n - \boldsymbol{\mu}_{n-1} &= -\Delta t \nabla_{\boldsymbol{y}} \mathcal{H}(\boldsymbol{y}_n, \boldsymbol{\lambda}_n, \boldsymbol{u}_{n-1}, \boldsymbol{\mu}_{n-1}, \boldsymbol{\zeta}_{n-1}), \\
\mathbf{0} &= \nabla_{\boldsymbol{\lambda}} \mathcal{H}(\boldsymbol{y}_n, \boldsymbol{\lambda}_n, \boldsymbol{u}_{n-1}, \boldsymbol{\mu}_{n-1}, \boldsymbol{\zeta}_{n-1}), \\
\mathbf{0} &= \nabla_{\boldsymbol{\zeta}} \mathcal{H}(\boldsymbol{y}_n, \boldsymbol{\lambda}_n, \boldsymbol{u}_{n-1}, \boldsymbol{\mu}_{n-1}, \boldsymbol{\zeta}_{n-1}), \\
\mathbf{0} &= \nabla_{\boldsymbol{u}} \mathcal{H}(\boldsymbol{y}_n, \boldsymbol{\lambda}_n, \boldsymbol{u}_{n-1}, \boldsymbol{\mu}_{n-1}, \boldsymbol{\zeta}_{n-1}),
\end{aligned}$$

for $n = 1, 2, \cdots, N$, with transversality conditions

$$\begin{aligned}
\mathbf{0} &= \gamma \boldsymbol{g}_T(\boldsymbol{y}_N) \\
\mathbf{0} &= \gamma \nabla_{\boldsymbol{y}_N} \boldsymbol{g}_T(\boldsymbol{y}_N)^T \boldsymbol{\eta} + \beta_T \nabla_{\boldsymbol{y}_N} \psi(\boldsymbol{y}_N) - \boldsymbol{\mu}_N,
\end{aligned}$$

and initial conditions

$$\begin{aligned}
\boldsymbol{g}_0(\boldsymbol{y}_0) &= \mathbf{0}, \\
\boldsymbol{\mu}_0 + \nabla_{\boldsymbol{y}_0} \boldsymbol{g}_0(\boldsymbol{y}_0)^{\mathsf{T}} \boldsymbol{\nu} &= \mathbf{0}.
\end{aligned}$$

Box 1: SE1 time Integration Scheme for HBVP

The preservation of the discrete momentum map by the SE1 scheme for the mechanical control system has been demonstrated elsewhere [4, 40], and therefore the proof is omitted here. Now we express the direct approach for constrained mechanical control system and its equivalence with the indirect approach in the sense of [4, 40]. A direct corollary of this would be that the findings of

this study equally apply to both direct and indirect approaches. We proceed with the following minimisation problem (with $n = 1, \cdots, N$)

$$\begin{aligned} &\min_{\mathbf{y},\mathbf{u}} \mathcal{J}_\Delta(\mathbf{y},\mathbf{u}) \\ &\text{s.t., } \boldsymbol{y}_n - \boldsymbol{y}_{n-1} = \boldsymbol{f}_\Delta(\boldsymbol{y}_n, \boldsymbol{\lambda}_n, \boldsymbol{u}_{n-1}) \\ &\quad \boldsymbol{\Phi}_\Delta(\boldsymbol{y}_n) = \mathbf{0} \\ &\quad \gamma \boldsymbol{g}_T(\boldsymbol{y}_N) = \mathbf{0} \\ &\quad \boldsymbol{g}_0(\boldsymbol{y}_0) = \mathbf{0} \end{aligned} \tag{17}$$

where notation Δ represents the discrete counterpart of continuous function. The discrete running cost $\mathcal{L}_\Delta$, discrete forcing $\boldsymbol{f}_\Delta$ and discrete holonomic constraint $\boldsymbol{\Phi}_\Delta(\boldsymbol{y}_n)$ are evaluated at $(\boldsymbol{y}_n, \boldsymbol{\lambda}_n, \boldsymbol{u}_{n-1})$, and the discrete functions are defined as

$$\mathcal{L}_\Delta(\boldsymbol{y}_n, \boldsymbol{u}_{n-1}) := \Delta t \mathcal{L}(\boldsymbol{y}_n, \boldsymbol{u}_{n-1}), \tag{18}$$

$$\boldsymbol{f}_\Delta(\boldsymbol{y}_n, \boldsymbol{\lambda}_n, \boldsymbol{u}_{n-1}) := \Delta t \boldsymbol{f}(\boldsymbol{y}_n, \boldsymbol{\lambda}_n, \boldsymbol{u}_{n-1}), \tag{19}$$

$$\boldsymbol{\Phi}_\Delta(\boldsymbol{y}_n) := \Delta t \boldsymbol{\Phi}_q(\boldsymbol{y}_n), \tag{20}$$

with discrete cost functional

$$\mathcal{J}_\Delta(\mathbf{y},\mathbf{u}) := \beta_T \psi(\boldsymbol{y}_N) + \sum_{n=1}^{N} \mathcal{L}_\Delta(\boldsymbol{y}_n, \boldsymbol{u}_{n-1}).$$

Next, we introduce adjoint variables $\boldsymbol{\mu} = (\boldsymbol{\mu}_0, \cdots, \boldsymbol{\mu}_N), \boldsymbol{\zeta} = (\boldsymbol{\zeta}_0, \cdots, \boldsymbol{\zeta}_{N-1})$, and $\boldsymbol{\eta}$, and define the control Hamiltonian $\mathcal{H}_\Delta$ associated with direct OCP-DAE in Eq (17) as

$$\mathcal{H}_\Delta(\boldsymbol{y}_n, \boldsymbol{\lambda}_n, \boldsymbol{\mu}_{n-1}, \boldsymbol{u}_{n-1}, \boldsymbol{\zeta}_{n-1}) = \mathcal{L}_\Delta(\boldsymbol{y}_n, \boldsymbol{u}_{n-1}) + \boldsymbol{\mu}_{n-1}^\mathsf{T} \boldsymbol{f}_\Delta(\boldsymbol{y}_n, \boldsymbol{\lambda}_n, \boldsymbol{u}_{n-1}) + \boldsymbol{\zeta}_{n-1}^\mathsf{T} \boldsymbol{\Phi}_\Delta(\boldsymbol{y}_n). \tag{21}$$

We adjoin the constraints with the cost functional $\mathcal{J}_\Delta$ and define discrete Lagrangian function

$$\mathcal{S}_\Delta = \sum_{n=1}^{N} \mathcal{H}_\Delta(\boldsymbol{y}_n, \boldsymbol{\lambda}_n, \boldsymbol{\mu}_{n-1}, \boldsymbol{u}_{n-1}, \boldsymbol{\zeta}_{n-1}) - \boldsymbol{\mu}_{n-1}^T(\boldsymbol{y}_n - \boldsymbol{y}_{n-1}) + \beta_T \psi(\boldsymbol{y}_N) + \gamma \boldsymbol{\eta}^\mathsf{T} \boldsymbol{g}_T(\boldsymbol{y}_N) - \boldsymbol{\mu}_0^\mathsf{T} \boldsymbol{g}_0(\boldsymbol{y}(0)). \tag{22}$$

Then for evaluation point $(\boldsymbol{y}_n, \boldsymbol{\lambda}_n, \boldsymbol{u}_{n-1}, \boldsymbol{\mu}_{n-1}, \boldsymbol{\zeta}_{n-1})$, first-variation of discrete Lagrangian $\mathcal{S}_\Delta$ results in exactly same NLP as shown in the Box 1. Appendix C deduces these expressions for the direct approach, and also for more general time-integrations schemes than SE1.

5 Monolithic and staggered FBSM solution approaches

In the sequel, we present the monolithic solver and the staggered Forward-Backward Sweep Method (FBSM) for the numerical solution of the nonlinear programming problem (NLP) associated with integration scheme SE1. In particular, we resort to a Newton-based strategies for both solution approaches. We propose an efficient implementation of an staggered algorithm (FBSM-Newton) which enjoys the quadratic convergence rate and satisfies feasibility of Newton tolerances below 10^{-9}. In order to further reduce the solution time, we additionally propose hybrid solution strategies that combine FBSM using gradient-based updates (FBSM-gradient), and each one of the two previous strategies, monolithic and FBSM-Newton.

5.1 Monolithic solver

Concerning the implementation of a Newton-based solver for integration scheme SE1, it is convenient to introduce the global residual vector $\boldsymbol{r}(\boldsymbol{w})$ as a function of vector $\boldsymbol{w}$ defined as $\boldsymbol{w} = (\boldsymbol{\mu}, \boldsymbol{\zeta}, \mathbf{y}, \boldsymbol{\lambda}, \boldsymbol{\eta}, \mathbf{u})$, where $\boldsymbol{\mu} = (\boldsymbol{\mu}_0, \ldots, \boldsymbol{\mu}_N)$, $\mathbf{y} = (\boldsymbol{y}_1, \ldots, \boldsymbol{y}_N)$, $\mathbf{u} = (\boldsymbol{u}_0, \ldots, \boldsymbol{u}_{N-1})$, $\boldsymbol{\lambda} = (\boldsymbol{\lambda}_1, \ldots, \boldsymbol{\lambda}_N)$, and $\boldsymbol{\zeta} = (\boldsymbol{\zeta}_0, \ldots, \boldsymbol{\zeta}_{N-1})$. Then the residual vector reads (where $n = 1, \cdots, N$ and blue lines show the partition of the residual vector into the adjoint equations, state equations, state final condition and control

equations)

$$\boldsymbol{r}_w(\boldsymbol{w}) = \left[\begin{array}{c} \vdots \\ \Delta t \nabla_{\boldsymbol{y}} \mathcal{H}(\boldsymbol{y}_n, \boldsymbol{\lambda}_n, \boldsymbol{u}_{n-1}, \boldsymbol{\mu}_{n-1}, \boldsymbol{\zeta}_{n-1}) + \boldsymbol{\mu}_n - \boldsymbol{\mu}_{n-1} \\ \vdots \\ \beta_T \nabla_{\boldsymbol{y}_N} \psi(\boldsymbol{y}_N) + \gamma \nabla_{\boldsymbol{y}_N} \boldsymbol{g}_T(\boldsymbol{y}_N)^T \boldsymbol{\eta} - \boldsymbol{\mu}_N \\ \vdots \\ \nabla_{\boldsymbol{\lambda}} \mathcal{H}(\boldsymbol{y}_n, \boldsymbol{\lambda}_n, \boldsymbol{u}_{n-1}, \boldsymbol{\mu}_{n-1}, \boldsymbol{\zeta}_{n-1}) \\ \vdots \\ \hline \vdots \\ \Delta t \nabla_{\boldsymbol{\mu}} \mathcal{H}(\boldsymbol{y}_n, \boldsymbol{\lambda}_n, \boldsymbol{u}_{n-1}, \boldsymbol{\mu}_{n-1}, \boldsymbol{\zeta}_{n-1}) - \boldsymbol{y}_n + \boldsymbol{y}_{n-1} \\ \vdots \\ \nabla_{\boldsymbol{\zeta}} \mathcal{H}(\boldsymbol{y}_n, \boldsymbol{\lambda}_n, \boldsymbol{u}_{n-1}, \boldsymbol{\mu}_{n-1}, \boldsymbol{\zeta}_{n-1}) \\ \vdots \\ \hline \gamma \boldsymbol{g}_T(\boldsymbol{y}_N) \\ \hline \vdots \\ \nabla_{\boldsymbol{u}} \mathcal{H}(\boldsymbol{y}_n, \boldsymbol{\lambda}_n, \boldsymbol{u}_{n-1}, \boldsymbol{\mu}_{n-1}, \boldsymbol{\zeta}_{n-1}) \\ \vdots \end{array}\right]$$

Linearising the residual vector $\boldsymbol{r}_w(\boldsymbol{w})$ about $\boldsymbol{w}^k$ with $k \in \mathbb{N}_0$, we obtain the following update for the variable $\boldsymbol{w}^{k+1}$ along the Newton search direction $\boldsymbol{d}^k = -\left[\nabla_{\boldsymbol{w}} \boldsymbol{r}_w(\boldsymbol{w}^k)\right]^{-1} \boldsymbol{r}_w(\boldsymbol{w}^k)$ [33]

$$\boldsymbol{w}^{k+1} = \boldsymbol{w}^k + \boldsymbol{d}^k, \tag{23}$$

supplemented with a suitable initial guess $\boldsymbol{w}^0$. In general, deducing a close/analytical form of Jacobian $\nabla_{\boldsymbol{w}} \boldsymbol{r}_w$ is a cumbersome task, error-prone and often unavailable. In this work, the Jacobian is obtained from the finite-difference approximation. Finally, the variables are updated until the Euclidean norm of residual vector $\|\boldsymbol{r}_w^{k+1}\|$ and incremental change in the variables $\|\boldsymbol{w}^{k+1} - \boldsymbol{w}^k\|$ fall below 10^{-9}.

5.2 Staggered FBSM solver

Recall that the optimality conditions constitute a two-point HBVP with a prescribed initial state $\boldsymbol{y}_0$ and adjoint state at the final time $\boldsymbol{\mu}_N$, cf. HBVP (12a). In a conventional staggered solution procedure such as the Forward-Backward Sweep Method [29]), optimality conditions are integrated separately following the flow of state and adjoint ODE/DAEs. Here the central idea is that given admissible control history $\mathbf{u}^k \in \mathcal{U}$ and initial state $\boldsymbol{y}_0$, one can integrate the state equations forward in time to obtain the admissible system state history $(\mathbf{y}, \boldsymbol{\lambda})$ [18, 25, 32]. Since the adjoint equations only require the admissible control and state trajectory, the adjoint history $(\boldsymbol{\mu}, \boldsymbol{\zeta})$ can be populated by integrating the adjoint equations backwards in time, starting with the prescribed final condition for $\boldsymbol{\mu}_N$. The thus obtained admissible tuplet $(\mathbf{u}^k, \mathbf{y}^k, \boldsymbol{\lambda}^k, \boldsymbol{\mu}^k, \boldsymbol{\zeta}^k)$ can be used to iteratively update the control signal $\mathbf{u}^{k+1} = \mathbf{u}^k + \gamma_o^k \boldsymbol{c}^k$ by taking a suitable step-size γ_o^k along search/descent direction $\boldsymbol{c}^k$ in accordance with the control residual [11, 12]. This solution procedure is often convergent provided an adequate step size is considered and the ODE-state system can be integrated into a staggered fashion. However, the major challenge with the OCPs having prescribed initial and final states $(\boldsymbol{y}_0, \boldsymbol{y}_N)$ is that the optimality conditions include boundary conditions for adjoints at the final time $(\boldsymbol{\mu}_N)$, which depend on an unknown multiplier $\boldsymbol{\eta}$ that enforces the end condition (see Remark 2). In this case, the adjoint $\boldsymbol{\eta}$ is included in the update step jointly with control variable $\mathbf{u}$. In Section 5.2.2 we also describe an alternative approach for solving the final state constraints with some extra adjoint variables.

5.2.1 Newton-based Staggered FBSM with final state constraints (FBSM-Newton)

In view of expression of the Hamiltonian $\mathcal{H}$ in (11), the SE1 time integration scheme in Box 1 can be written as

$$\Delta t \boldsymbol{f}(\boldsymbol{y}_n, \boldsymbol{\lambda}_n, \boldsymbol{u}_{n-1}) - \boldsymbol{y}_n + \boldsymbol{y}_{n-1} = \mathbf{0} \tag{24}$$

$$\boldsymbol{\Phi}_q(\boldsymbol{y}_n) = \mathbf{0} \tag{25}$$

$$\boldsymbol{\mu}_n - \boldsymbol{\mu}_{n-1} + \Delta t \nabla_{\boldsymbol{y}} \boldsymbol{f}(\boldsymbol{y}_n, \boldsymbol{\lambda}_n, \boldsymbol{u}_{n-1})^{\mathsf{T}} \boldsymbol{\mu}_{n-1} + \Delta t \nabla_{\boldsymbol{y}} \boldsymbol{\Phi}_q(\boldsymbol{y}_n)^{\mathsf{T}} \boldsymbol{\zeta}_{n-1} + \Delta t \nabla_{\boldsymbol{y}} \mathcal{L}(\boldsymbol{y}_n, \boldsymbol{u}_{n-1}) = \mathbf{0} \tag{26}$$

$$\nabla_{\boldsymbol{\lambda}} \boldsymbol{f}(\boldsymbol{y}_n, \boldsymbol{\lambda}_n, \boldsymbol{u}_{n-1})^{\mathsf{T}} \boldsymbol{\mu}_{n-1} = \mathbf{0} \tag{27}$$

$$\nabla_u \mathcal{L}(\boldsymbol{y}_n, \boldsymbol{u}_{n-1}) + \nabla_u \boldsymbol{f}(\boldsymbol{y}_n, \boldsymbol{\lambda}_n, \boldsymbol{u}_{n-1})^{\mathsf{T}} \boldsymbol{\mu}_{n-1} = \mathbf{0} \tag{28}$$

with end conditions $\boldsymbol{y}(0) = \boldsymbol{y}_0, \boldsymbol{g}_T(\boldsymbol{y}_N) = \mathbf{0}$ and $\boldsymbol{\mu}_N = \beta_T \nabla_{\boldsymbol{y}_N} \psi(\boldsymbol{y}_N) + \gamma \nabla_{\boldsymbol{y}_N} \boldsymbol{g}(\boldsymbol{y}_N)^{\mathsf{T}} \boldsymbol{\eta}$. A conventional staggered FBSM solver can be constructed as follows (say $\boldsymbol{\omega} = (\boldsymbol{\eta}, \mathbf{u})$ with $\mathbf{u} = (\boldsymbol{u}_0, \ldots, \boldsymbol{u}_{N-1})$) [13, 29]

1. **Initial guess**: Give initial history $\boldsymbol{\omega}^0 = (\boldsymbol{\eta}^0, \mathbf{u}^0)$
2. **State DAEs: forward integration**: Given $\mathbf{u}^k$ and initial conditions $\boldsymbol{y}(0) = \boldsymbol{y}_0$, integrate the system of non-linear equations for $n = 1, \cdots, N$

$$\begin{aligned} \Delta t \boldsymbol{f}(\boldsymbol{y}_n, \boldsymbol{\lambda}_n, \boldsymbol{u}_{n-1}) - \boldsymbol{y}_n + \boldsymbol{y}_{n-1} &= \mathbf{0} \\ \boldsymbol{\Phi}_q(\boldsymbol{y}_n) &= \mathbf{0} \end{aligned}$$

   In each time step, the resulting algebraic system can be solved by applying the Newton-Raphson method: given $(\boldsymbol{y}_{n-1}, \boldsymbol{\lambda}_{n-1})$, the state variables $(\boldsymbol{y}_n, \boldsymbol{\lambda}_n)$ are obtained by iteratively solving

$$\begin{bmatrix} \Delta t \nabla_{\boldsymbol{y}} \boldsymbol{f}(\boldsymbol{y}_n, \boldsymbol{\lambda}_n, \boldsymbol{u}_{n-1}) - \mathbf{I} & \Delta t \nabla_{\boldsymbol{\lambda}} \boldsymbol{f}(\boldsymbol{y}_n, \boldsymbol{\lambda}_n, \boldsymbol{u}_{n-1}) \\ \nabla_{\boldsymbol{y}} \boldsymbol{\Phi}_q(\boldsymbol{y}_n)^{\mathsf{T}} & \mathbf{0} \end{bmatrix} \begin{bmatrix} \delta \boldsymbol{y}_n \\ \delta \boldsymbol{\lambda}_n \end{bmatrix} = - \begin{bmatrix} \Delta t \boldsymbol{f}(\boldsymbol{y}_n, \boldsymbol{\lambda}_n, \boldsymbol{u}_{n-1}) - \boldsymbol{y}_n + \boldsymbol{y}_{n-1} \\ \boldsymbol{\Phi}_q(\boldsymbol{y}_n) \end{bmatrix} \tag{29}$$

   and update $(\boldsymbol{y}_n, \boldsymbol{\lambda}_n) \to (\boldsymbol{y}_n + \delta \boldsymbol{y}_n, \boldsymbol{\lambda}_n + \delta \boldsymbol{\lambda}_n)$.
3. **Adjoint DAEs: backward integration**: Given $\mathbf{u}^k, \boldsymbol{\eta}^k, \mathbf{y}^k, \boldsymbol{\lambda}^k$, with the transversality conditions $\boldsymbol{\mu}_N = \beta_T \nabla_{\boldsymbol{y}_N} \psi(\boldsymbol{y}_N) + \gamma \nabla_{\boldsymbol{y}_N} \boldsymbol{g}(\boldsymbol{y}_N)^{\mathsf{T}} \boldsymbol{\eta}^k$, integrate adjoint DAEs backward in time. That is, for $n = N, N-1, \ldots, 1$,

$$\begin{bmatrix} \Delta t \nabla_{\boldsymbol{y}} \boldsymbol{f}(\boldsymbol{y}_n, \boldsymbol{\lambda}_n, \boldsymbol{u}_{n-1})^{\mathsf{T}} - \mathbf{I} & \Delta t \nabla_{\boldsymbol{y}} \boldsymbol{\Phi}_q(\boldsymbol{y}_n)^{\mathsf{T}} \\ \nabla_{\boldsymbol{\lambda}} \boldsymbol{f}(\boldsymbol{y}_n, \boldsymbol{\lambda}_n, \boldsymbol{u}_{n-1})^{\mathsf{T}} & \mathbf{0} \end{bmatrix} \begin{bmatrix} \boldsymbol{\mu}_{n-1} \\ \boldsymbol{\zeta}_{n-1} \end{bmatrix} = - \begin{bmatrix} \Delta t \nabla_{\boldsymbol{y}} \mathcal{L}(\boldsymbol{y}_n, \boldsymbol{u}_{n-1}) + \boldsymbol{\mu}_n \\ \mathbf{0} \end{bmatrix} \tag{30}$$

   and update adjoint history $\boldsymbol{\mu}^k$ and $\boldsymbol{\zeta}^k$.
4. **Control update** given $\boldsymbol{\omega}^k = (\boldsymbol{\eta}^k, \mathbf{u}^k), \mathbf{y}^k, \boldsymbol{\lambda}^k, \boldsymbol{\mu}^k, \boldsymbol{\zeta}^k$, update $\boldsymbol{\omega}^{k+1} = \boldsymbol{\omega}^k + \gamma_o^k \boldsymbol{c}^k$, by moving with step-size γ_o^k along the search direction $\boldsymbol{c}^k$ which minimises the residual $\boldsymbol{r}_u$ defined by

$$\boldsymbol{r}_u(\boldsymbol{\omega}) = \left[\begin{array}{c} \boldsymbol{\gamma} \boldsymbol{g}_T(\boldsymbol{y}_N) \\ \hline \vdots \\ \nabla_{\boldsymbol{u}} \mathcal{H}(\boldsymbol{y}_n, \boldsymbol{\lambda}_n, \boldsymbol{u}_{n-1}, \boldsymbol{\mu}_{n-1}, \boldsymbol{\zeta}_{n-1}) \\ \vdots \\ \nabla_{\boldsymbol{u}} \mathcal{H}(\boldsymbol{y}_N, \boldsymbol{\lambda}_N, \boldsymbol{u}_{N-1}, \boldsymbol{\mu}_{N-1}, \boldsymbol{\zeta}_{N-1}) \end{array} \right], \tag{31}$$

   and continue with step 2 until the convergence criteria are met.

The convergence rate of the posed conventional FBSM relies heavily on the choice of line search scheme and search direction. Conventional FBSM approaches employ descent directions $\boldsymbol{c}^k = -\boldsymbol{r}_u(\boldsymbol{\omega}^k)$ as search space and an inexact line search strategy with an accelerator to estimate adequate step length γ_o^k, which results in a sufficient decrease of the objective functional [13, 29]. These gradient-based schemes with suitable accelerators initially perform quite well even with a poor initial guess. However, they significantly slow down near extrema. Furthermore, inexact line search often introduces too many backtracking operations and hinders the performance of staggered solver. Considering this, we provide an alternate implementation of FBSM in the reduced space spanned by $\boldsymbol{\omega}$ to minimise the residual $\boldsymbol{r}_u(\boldsymbol{\omega})$ along Newton's search direction, which we denote by FBSM-Newton.

Suppose that we start with some suitable $\boldsymbol{\omega}^k$ at iteration $k \in \mathbb{N}_0$. Then, as shown above, we can easily obtain state and adjoint trajectories by applying forward and backward integration of state and adjoint DAEs, respectively. In other words, the residual is a sole function of independent variable $\boldsymbol{u}$ and $\boldsymbol{\eta}$. Linearising the residual $\boldsymbol{r}_u(\boldsymbol{\omega})$ about $\boldsymbol{\omega}^k$, this leads to the following update for the $\boldsymbol{\omega}^{k+1}$ along the Newton search direction $\boldsymbol{c}^k = -\left[\nabla_{\boldsymbol{\omega}} \boldsymbol{r}_u(\boldsymbol{\omega}^k)\right]^{-1} \boldsymbol{r}_u(\boldsymbol{\omega}^k)$

$$\boldsymbol{\omega}^{k+1} = \boldsymbol{\omega}^k + \gamma_o^k \boldsymbol{c}^k, \tag{32}$$

where we first attempt $\gamma_o^k = 1$, provided this results in the reduction of the residual compared to the previous value, i.e, $\|\boldsymbol{r}_u(\boldsymbol{\omega}^{k+1})\| < \|\boldsymbol{r}_u(\boldsymbol{\omega}^k\|)$ is fulfilled. Otherwise, we perform backtracking along $\boldsymbol{c}^k$ by halving the step length ($\gamma_o^k \to \gamma_o^k/2$) until the above condition is satisfied or we exceed the maximum of $i_{\max} := 10$ allowed bisections. Since the Newton search directions are descent, the existence of such a step can be ensured although it may require too many bisections which we therefore limited to 10, which is often sufficient in practical applications. Hessian $\mathbf{K} := \nabla_{\boldsymbol{\omega}} \boldsymbol{r}_u(\boldsymbol{\omega})$ is built with the finite-difference approximation and variables are updated until the Euclidean norm of residual, $\|\boldsymbol{r}_u^{k+1}\|$, and incremental change in variables, $\|\boldsymbol{\omega}^{k+1} - \boldsymbol{\omega}^k\|$, fall below $tol := 10^{-9}$. The implementation of the staggered FBSM-Newton solver is summarised in Algorithm 1.

Algorithm 1 Staggered FBSM combined with Newton line-search (FBSM-Newton).

Set $k = 0, tol = 10^{-9}, i_{max} = 10, err = \infty, \mathbf{u}^0, \boldsymbol{\eta}^0$
$\boldsymbol{\omega}^0 = (\boldsymbol{\eta}^0, \mathbf{u}^0)$
$\boldsymbol{r}_u^0 = \text{RESIDUE}(\boldsymbol{\omega}^0)$
$\mathbf{K} = \text{JACOBIAN}(\boldsymbol{r}_u^0, \boldsymbol{\omega}^0)$ ▷ Numerical Jacobian
while $err > tol$ **do**
  $\boldsymbol{c}^k = -\mathbf{K}^{-1}\boldsymbol{r}_u^k$ ▷ Initial search direction
  $\gamma_o^k = 1, i = 1, \Delta = \infty$
  while $\Delta > \text{eps} \quad \& \quad i \leq i_{\max}$ **do** ▷ Ensuring minimization
    $\boldsymbol{\omega}^{k+1} \leftarrow \boldsymbol{\omega}^k + \gamma_o^k \boldsymbol{c}^k$
    $\boldsymbol{r}_u^{k+1} = \text{RESIDUE}(\boldsymbol{\omega}^{k+1})$ ▷ Update residue
    $\Delta = ||\boldsymbol{r}_u^{k+1}|| - ||\boldsymbol{r}_u^k||$
    $\gamma_o^k = \frac{\gamma_o^k}{2}$ ▷ Back tracking
    $i = i + 1$
  end while
  $err \leftarrow \max\{||\boldsymbol{r}_u^{k+1}||, ||\boldsymbol{\omega}^{k+1} - \boldsymbol{\omega}^k||\}$
  if $err > tol$ **then**
    $\mathbf{K} = \text{JACOBIAN}(\boldsymbol{r}_u^{k+1}, \boldsymbol{\omega}^{k+1})$ ▷ Numerical Jacobian
  end if
  $k \leftarrow k + 1$
end while
return $\mathbf{u}^*, \mathbf{y}^*, \mathcal{J}^*$ ▷ Optimal solution

function $\boldsymbol{r}_u = \text{RESIDUE}(\boldsymbol{\omega})$
  $(\boldsymbol{\eta}, \mathbf{u}) \leftarrow \boldsymbol{\omega}$
  $(\mathbf{y}, \boldsymbol{\lambda}) = \text{State}(\mathbf{u}, \boldsymbol{y}_0)$ ▷ Solve state DAEs forward in time, cf. Eq (29)
  $(\boldsymbol{\mu}, \boldsymbol{\zeta}) = \text{Adjoint}(\mathbf{u}, \boldsymbol{\eta}, \mathbf{y}, \boldsymbol{\lambda})$ ▷ Solve adjoint DAEs backward in time, cf. Eq (30)
  return $\boldsymbol{r}_u(\mathbf{u}, \mathbf{y}, \boldsymbol{\mu})$ ▷ Evaluate residual Eq (31)
end function

5.2.2 Use of auxiliary adjoint variables in the presence of final state constraints

One alternative to handle the presence of prescribed initial and final states $(\boldsymbol{y}_0, \boldsymbol{y}_N)$ is to split the adjoint variables into homogeneous and inhomogeneous terms and adapt the equations in the previous adjoint solution technique. This approach is introduced in [18] for minimal-time OCPs and indeed is an effective way to preserve the structure of a conventional staggered FBSM solver. Following [18], this split is fulfilled by introducing two additional adjoint variables viz a vector $\boldsymbol{\sigma}(t)$ and matrix $\mathbf{A}(t)$ such that

$$\boldsymbol{\mu}(t) := \boldsymbol{\sigma}(t) + \mathbf{A}(t)\boldsymbol{\eta} \tag{33}$$

where $\boldsymbol{\eta}$ is the multiplier used to enforce $\boldsymbol{g}_T(\boldsymbol{y}_N)$ as described in Section 3.1. Substituting Eq (33) into the adjoint DAEs (see Eq (12a)), auxiliary adjoint equations and boundary term result in

$$\left(\dot{\boldsymbol{\sigma}} + \nabla_{\boldsymbol{y}}\boldsymbol{f}^{\mathsf{T}}\boldsymbol{\sigma} + \nabla_{\boldsymbol{y}}\boldsymbol{\Phi}^{\mathsf{T}}\boldsymbol{\zeta} + \nabla_{\boldsymbol{y}}\mathcal{L}\right) + \left(\dot{\mathbf{A}} + \nabla_{\boldsymbol{y}}\boldsymbol{f}^{\mathsf{T}}\mathbf{A}\right)\boldsymbol{\eta} = \mathbf{0} \tag{34}$$

$$\left(\beta_T \nabla_{\boldsymbol{y}(T)}\psi(\boldsymbol{y}(T)) - \boldsymbol{\sigma}(T)\right) + \left(\gamma \nabla_{\boldsymbol{y}(T)}\boldsymbol{g}_T(\boldsymbol{y}(T))^{\mathsf{T}} - \mathbf{A}(T)\right)\boldsymbol{\eta} = \mathbf{0} \tag{35}$$

$$\nabla_{\boldsymbol{\lambda}}\boldsymbol{f}^{\mathsf{T}}\boldsymbol{\sigma} + \nabla_{\boldsymbol{\lambda}}\boldsymbol{f}^{\mathsf{T}}\mathbf{A}\boldsymbol{\eta} = \mathbf{0} \tag{36}$$

Since the adjoint variables $\boldsymbol{\mu}(t)$ in (33) are now represented by the new quantities $\boldsymbol{\sigma}(t)$ and $\mathbf{A}(t)$, the matrix adjoint variables $\mathbf{A}(t)$ can be viewed as additional degrees of freedom. We now require $\mathbf{A}(t)$ to satisfy the matrix-differential equation

$$\dot{\mathbf{A}} + \nabla_{\boldsymbol{y}}\boldsymbol{f}^{\mathsf{T}}\mathbf{A} = \mathbf{0},$$

along with the terminal condition $\mathbf{A}(T) = \gamma \nabla_{\boldsymbol{y}(T)}\boldsymbol{g}_T(\boldsymbol{y}(T))^{\mathsf{T}}$. This is equivalent to setting the terms in the parenthesis in front of multiplier $\boldsymbol{\eta}$ in Eq (34) and Eq (35) to zero, which results in the following set of adjoint vector and matrix differential equations

$$\dot{\boldsymbol{\sigma}} + \nabla_{\boldsymbol{y}}\boldsymbol{f}^{\mathsf{T}}\boldsymbol{\sigma} + \nabla_{\boldsymbol{y}}\boldsymbol{\Phi}^{\mathsf{T}}\boldsymbol{\zeta} + \nabla_{\boldsymbol{y}}\mathcal{L} = \mathbf{0}, \quad \boldsymbol{\sigma}(T) = \beta_T \nabla_{\boldsymbol{y}(T)}\psi(\boldsymbol{y}(T)) \tag{37}$$

$$\dot{\mathbf{A}} + \nabla_{\boldsymbol{y}}\boldsymbol{f}^{\mathsf{T}}\mathbf{A} = \mathbf{0}, \quad \mathbf{A}(T) = \gamma \nabla_{\boldsymbol{y}(T)}\boldsymbol{g}_T(\boldsymbol{y}(T))^{\mathsf{T}} \tag{38}$$

$$\nabla_{\boldsymbol{\lambda}}\boldsymbol{f}^{\mathsf{T}}\boldsymbol{\sigma} + \nabla_{\boldsymbol{\lambda}}\boldsymbol{f}^{\mathsf{T}}\mathbf{A}\boldsymbol{\eta} = \mathbf{0}. \tag{39}$$

As discussed in Remark 3, for the Lagrange OCP-DAE ($\gamma = 1, \beta_T = 0$), it is necessary to reduce the boundary conditions since constraints are active at the final time. This is equivalent to imposing $\mathbf{A}(T) = \mathbf{D}^{\mathsf{T}}$ and $\boldsymbol{g}_T(\boldsymbol{y}(T)) = \mathbf{D}(\boldsymbol{y}_N - \boldsymbol{y}_d)$, with $\mathbf{D}$ defined after Eq (14).

For OCP-ODE, we ignore Eq (39) and impose $\boldsymbol{\lambda} = \boldsymbol{\zeta} = \mathbf{0}$ in Eq (37) and Eq (38). This leads to the following adjoint ODEs for the OCP-ODE problem (see Example 6.1)

$$\dot{\boldsymbol{\sigma}} + \nabla_{\boldsymbol{y}}\boldsymbol{f}^{\mathsf{T}}\boldsymbol{\sigma} + \nabla_{\boldsymbol{y}}\mathcal{L} = \mathbf{0}, \quad \boldsymbol{\sigma}(T) = \beta_T \nabla_{\boldsymbol{y}(T)}\psi(\boldsymbol{y}(T)) \tag{40}$$

$$\dot{\mathbf{A}} + \nabla_{\boldsymbol{y}}\boldsymbol{f}^{\mathsf{T}}\mathbf{A} = \mathbf{0}, \quad \mathbf{A}(T) = \gamma \nabla_{\boldsymbol{y}(T)}\boldsymbol{g}_T(\boldsymbol{y}(T))^{\mathsf{T}}. \tag{41}$$

The time discretisation of the ODEs in (37), (38), and (39) with SE1 algorithm yields the following system of equations ($n = N, N-1, \cdots, 1$):

$$\mathbf{A}_n - \mathbf{A}_{n-1} + \Delta t \nabla_{\boldsymbol{y}}\boldsymbol{f}(\boldsymbol{y}_n, \boldsymbol{\lambda}_n, \boldsymbol{u}_{n-1})^{\mathsf{T}}\mathbf{A}_{n-1} = \mathbf{0} \tag{42}$$

$$\boldsymbol{\sigma}_n - \boldsymbol{\sigma}_{n-1} + \Delta t \nabla_{\boldsymbol{y}}\boldsymbol{f}(\boldsymbol{y}_n, \boldsymbol{\lambda}_n, \boldsymbol{u}_{n-1})^{\mathsf{T}}\boldsymbol{\sigma}_{n-1} + \Delta t \nabla_{\boldsymbol{y}}\boldsymbol{\Phi}(\boldsymbol{y}_n)^{\mathsf{T}}\boldsymbol{\zeta}_{n-1} + \Delta t \nabla_{\boldsymbol{y}}\mathcal{L}(\boldsymbol{y}_n, \boldsymbol{u}_{n-1}) = \mathbf{0} \tag{43}$$

$$\nabla_{\boldsymbol{\lambda}}\boldsymbol{f}(\boldsymbol{y}_n, \boldsymbol{\lambda}_n, \boldsymbol{u}_{n-1})^{\mathsf{T}}\boldsymbol{\sigma}_{n-1} + \nabla_{\boldsymbol{\lambda}}\boldsymbol{f}(\boldsymbol{y}_n, \boldsymbol{\lambda}_n, \boldsymbol{u}_{n-1})^{\mathsf{T}}\left(\mathbf{A}_{n-1}\boldsymbol{\eta}\right) = \mathbf{0}, \tag{44}$$

with transversality conditions $\boldsymbol{\sigma}_N = \beta_T \nabla_{\boldsymbol{y}_N}\psi(\boldsymbol{y}_N)$, $\mathbf{A}_N = \gamma \nabla_{\boldsymbol{y}_N}\boldsymbol{g}_T(\boldsymbol{y}_N)^{\mathsf{T}}$ and $\boldsymbol{\mu}_n = \boldsymbol{\sigma}_n + \mathbf{A}_n\boldsymbol{\eta}$. The implementation of this approach with auxiliary variables $\boldsymbol{\sigma}$ and $\mathbf{A}$ in our staggered FBSM algorithm requires the replacement of equation in (30) in the backward step with the equations in (42)-(44).

We remark that for given state $\boldsymbol{y}$ and control history $\boldsymbol{u}$, the adjoint matrix differential equation (38) can be integrated independently of the remaining two coupled DAEs (37) and (39). For OCP-ODE, the adjoint ODE in $\boldsymbol{\sigma}$ and $\mathbf{A}$ can be integrated independently.

5.3 Hybrid solver

The numerical solution of an NLP stemming from OCP is often difficult to converge and the convergence rate strongly depends upon the quality of the initial guess. The gradient-based method with a suitable accelerator performs quite well even with an initial guess which is very far from the extrema. However this approach typically becomes extremely slow near optima. On the contrary, the Hessian-based method converges quadratically near extrema, but poor initial guess may pose serious convergence issues. In addition to that, the computational effort associated with the Jacobian formation and inversion procedure might be quite high. Perhaps, the simplest idea would be to use key attributes

of both the gradient-based and Hessian-based methods. The proposed hybrid solver initially applies the staggered FBSM and updates the solution along the descent direction with Barzilai-Borwein line search [3], which we denote by FBSM-BB. After a few iterations the solution is updated by switching to a Hessian-based method, either monolithic or FBSM-Newton.

Accordingly, two hybrid strategies are proposed:

1. Start with some initial guess.
2. Use the gradient descent FBSM with Barzilai-Borwein linesearch, FBSM-BB, until $\|\boldsymbol{r}_u^{k+1}\| < 10$ or $\mathcal{J}^{k+1}$ reduces below 50% of its initial value $\mathcal{J}^0$, or the update exceeds the maximum allowed iterations. Store the solution.
3. Use the stored solution as starting point for applying one of the following strategies:
   (a) Apply the Newton-based monolithic solver as described in Section 5.1. Strategy **FBSM-BB + Monolithic.**
   (b) Apply the staggered solver as described in Section 5.2. Strategy **FBSM-BB + FBSM-Newton.**

6 Numerical Examples

We present three numerical examples to study the performance of monolithic, staggered FBSM-Newton, and the two hybrid solution strategies. We deduce the control laws for each physical systems whose motion is governed by ODEs or DAEs. The first example, consisting of an optimal tracking problem of a 3D elastic pendulum, is introduced to benchmark the developed in-house Matlab code. In the second example, we present the optimal control of a spherical pendulum whose motion is governed by index-3 DAEs. Finally, we examine the challenging swing-up manoeuvre of an underactuated inverted rigid and elastic planar pendulum. All examples are solved with the SE1 time-integration scheme. Convergence is assumed when the residual falls below 10^{-9}.

6.1 3D elastic pendulum

Let us consider a particle having mass m confined by an elastic spring with stiffness k and reference length l_o. To analyse the system, we fix a coordinate system at the origin 'O' (equipped with right-handed orthonormal vectors $\boldsymbol{E}_x, \boldsymbol{E}_y, \boldsymbol{E}_z$) with one end of the spring attached to it while the other end is tied to the particle. The configuration space of the system is $\mathcal{Q} = \mathbb{R}^3$ and is parametrised by Cartesian coordinates $\boldsymbol{q} = (q_x, q_y, q_z)$, denoting the spatial position of the particle (see Figure 1). Let $\boldsymbol{p} = (p_x, p_y, p_z)$ be the momenta of the particle measured w.r.t the origin and a denote the intensity of the gravitational force with potential energy $\mathcal{V}_a(\boldsymbol{q}) := ma\,\boldsymbol{q}\cdot\boldsymbol{E}_z$. The potential energy of the spring is assumed as a nonlinear function of current length $l = \sqrt{\boldsymbol{q}\cdot\boldsymbol{q}}$, given by $\mathcal{V}_e(\boldsymbol{q}) = \frac{k}{8l_o^2}\left(l(\boldsymbol{q})^2 - l_o^2\right)^2$ [4]. The total potential energy $\mathcal{V}(\boldsymbol{q}) := \mathcal{V}_e(\boldsymbol{q}) + \mathcal{V}_a(\boldsymbol{q})$ of the system is expressed as the sum of the elastic and gravitational potential energy. An additional control force $\boldsymbol{u} \in \mathbb{R}^3$ is applied to the particle to steer the system from the initial state to the desired final state. Then, the equations of motion are those in (1), and with no third block of equations due to the absence of holonomic constraints $\boldsymbol{\Phi}(\boldsymbol{q}) = \boldsymbol{0}$ and no Lagrange multipliers. The mechanical Hamiltonian $\mathcal{E}(\boldsymbol{q}, \boldsymbol{p})$ is accordingly given by

$$\mathcal{E}(\boldsymbol{q}, \boldsymbol{p}) = \frac{1}{2m}\boldsymbol{p}\cdot\boldsymbol{p} + \mathcal{V}(\boldsymbol{q}). \tag{45}$$

Introducing phase space coordinates $\boldsymbol{y} = (\boldsymbol{q}, \boldsymbol{p})$, we obtain our usual representation $\dot{\boldsymbol{y}} = \boldsymbol{f}(\boldsymbol{y}, \boldsymbol{u})$ (see Eq (2)). Assuming that the elastic pendulum system is controllable, we thus consider the optimal steering problem: find control function $\boldsymbol{u}(t)$ that steers the particle starting from initial state $\boldsymbol{y}(0) = \overline{\boldsymbol{y}}_0$ to the desired final state $\boldsymbol{y}(T) = \boldsymbol{y}_d$ in a given amount of time T, while minimizing the cost functional $\mathcal{J}(\boldsymbol{y}, \boldsymbol{u})$ in Eq (7). To benchmark the results obtained with different means to enforce the prescribed terminal state $\boldsymbol{y}(T) = \boldsymbol{y}_d$, we consider both Lagrange and penalty type OCP. As illustrated in [4] for $\mathcal{L}(\boldsymbol{u}) = \frac{\alpha}{2}\boldsymbol{u}\cdot\boldsymbol{u}$, the control Hamiltonian $\mathcal{H}(\boldsymbol{y}, \boldsymbol{u}; \boldsymbol{\mu}) = \mathcal{L}(\boldsymbol{u}) + \boldsymbol{\mu}\cdot\boldsymbol{f}(\boldsymbol{y}, \boldsymbol{u})$ is invariant to superimposed translations in time and superimposed rigid rotations about $\boldsymbol{E}_z$ (direction of gravity). Thus the optimal control problem possesses two integrals of motion, namely the control Hamiltonian $\mathcal{H}$ and a component of the control angular momentum given by $\xi_z = \boldsymbol{E}_z \cdot (\boldsymbol{q}\times\boldsymbol{\mu}^q + \boldsymbol{p}\times\boldsymbol{\mu}^p)$.

We solve the Lagrange problem with both the monolithic and the iterative approach. The following parameters correspond to [4, Section 5.1]: $T = 5$, $\alpha = 1$, $\gamma = 1$, $\beta = 0$, $\beta_T = 0$, $k = 0.6$, $m = 1$, $l_o = 5$, $a = 9.81$, $\overline{\boldsymbol{y}}_0 = (-2, -5, -5, -3, 0, 0)$, $\boldsymbol{y}_d = (2, -10, -4, 0, 0, 0)$, and we take $\Delta t = 0.01$. As initial guess we choose $\boldsymbol{u}(t) = 0.001$ at all time points, followed by solving the forward dynamics problem to generate admissible phase space coordinates.

The numerical results depicted in Figure 2 are in close agreement with those in [4]. As expected, the SE1 integrator is capable to preserve the control angular momentum about the gravity axis.

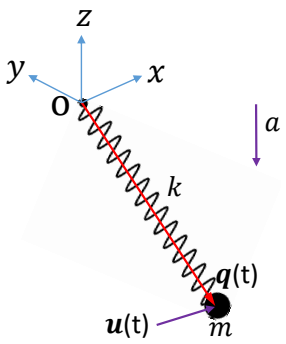

Figure 1: Schematic of 3d elastic pendulum.

Moreover, it turns out that both solvers under investigation show similar rates of convergence (see Table 1). This confirms that the newly proposed iterative strategy converges quadratically near extrema. We have tested the approach of Section 5.2.2 using auxiliary variables $\boldsymbol{\sigma}$ and $\mathbf{A}$. The number of iterations remained the same, and the CPU time was also similar, with a slight increase ($4786.9s$ instead of the 4516.84 seconds reported in Table 2 for $\Delta t = 0.01$).

Table 1: 3D elastic pendulum: Convergence of monolithic and staggered solver (Individual strategies, $\Delta t = 0.01$).

	Monolithic		**FBSM-Newton**	
Iteration	$\|\Delta \boldsymbol{w}\|_2$	$\|\boldsymbol{r}_w\|_2$	$\|\Delta \boldsymbol{\omega}\|_2$	$\|\boldsymbol{r}_u\|_2$
1	$3.823270e+02$	$3.586640e+02$	$1.712774e+01$	$1.256651e+01$
13	$2.189136e-03$	$1.435653e-08$	$2.312865e-03$	$5.544332e-08$
14	$1.034807e-08$	$1.967061e-12$	$5.518912e-08$	$3.213193e-13$
15	$1.890021e-14$	$2.004273e-12$	$2.891783e-13$	$2.465730e-13$

Next, we test the proposed penalty methodology to solve the minimal effort problem efficiently with prescribed initial and final states. Without altering other parameters, we choose, $\alpha = 10^{-3}$, $\gamma = 0$, $\beta_T = 1$. Since α appears in the control Hamiltonian (and eventually enters the control equation), straightforward computations show that the Control Hamiltonian and Lagrange multiplier of penalty problem $(\mathcal{H}^*, \boldsymbol{\mu}^*)$ differ by a factor of α from the Lagrange OCP Control Hamiltonian and multipliers $(\mathcal{H}, \boldsymbol{\mu})$ i.e., $\mathcal{H}^* = \alpha\mathcal{H}$ and $\boldsymbol{\mu}^* = \alpha\boldsymbol{\mu}$ (see Remark 2). These findings are verified with the numerical solution of penalty OCP by plotting the time evolution of $\boldsymbol{\mu}^*/\alpha$ and $\mathcal{H}^*/\alpha$ as depicted in Figure 2. It can also be observed from Figure 2 (g), that the algorithmic preservation of the control Hamiltonian is not achieved as discussed in Appendix B. Although, with the refinement of Δt, one can attain the constant reference value of 0.37 [4].

Finally, we study the performance of monolithic and iterative solvers with the increase in the size of the NLP. The first column of Table 2 indicates how the problem size (degrees of freedom (DOF)) increases, when the time steps Δt are refined. The second column of Table 2 shows the corresponding numerical costs of both the monolithic solver and FBSM. It can be observed that the monolithic solver performance is slowing down with the increase in DOF, although with fewer DOF there is no significant difference in the computational time of both solvers.

For comparison, we also include the results of the hybrid solution strategy (third column of Table 2). The hybrid approach relies on the following 2-step procedure: In the first step we apply the standard gradient-based approach to move along the descent direction by using the stabilised Barzilai-Borwein linesearch ($\theta_{max} = 1$, see [13]) for 25 iterations. In the second step we apply one of the methods at our disposal, namely either the monolithic solver or FBSM. The computational time of the hybrid strategy is reported in the third column of Table 2, where the total number of iterations is divided into gradient descent iterations (25) and individual solver iterations (6). Moreover, the CPU time in the Hybrid strategy for the monolithic and FBSM indicates the total time spent on the corresponding iterations for each strategy combined with the solution time corresponding to the gradient descent solver. One can clearly observe that the performance of the monolithic solver is drastically improved and convergence is achieved in just 6 iterations. Similarly, the improved

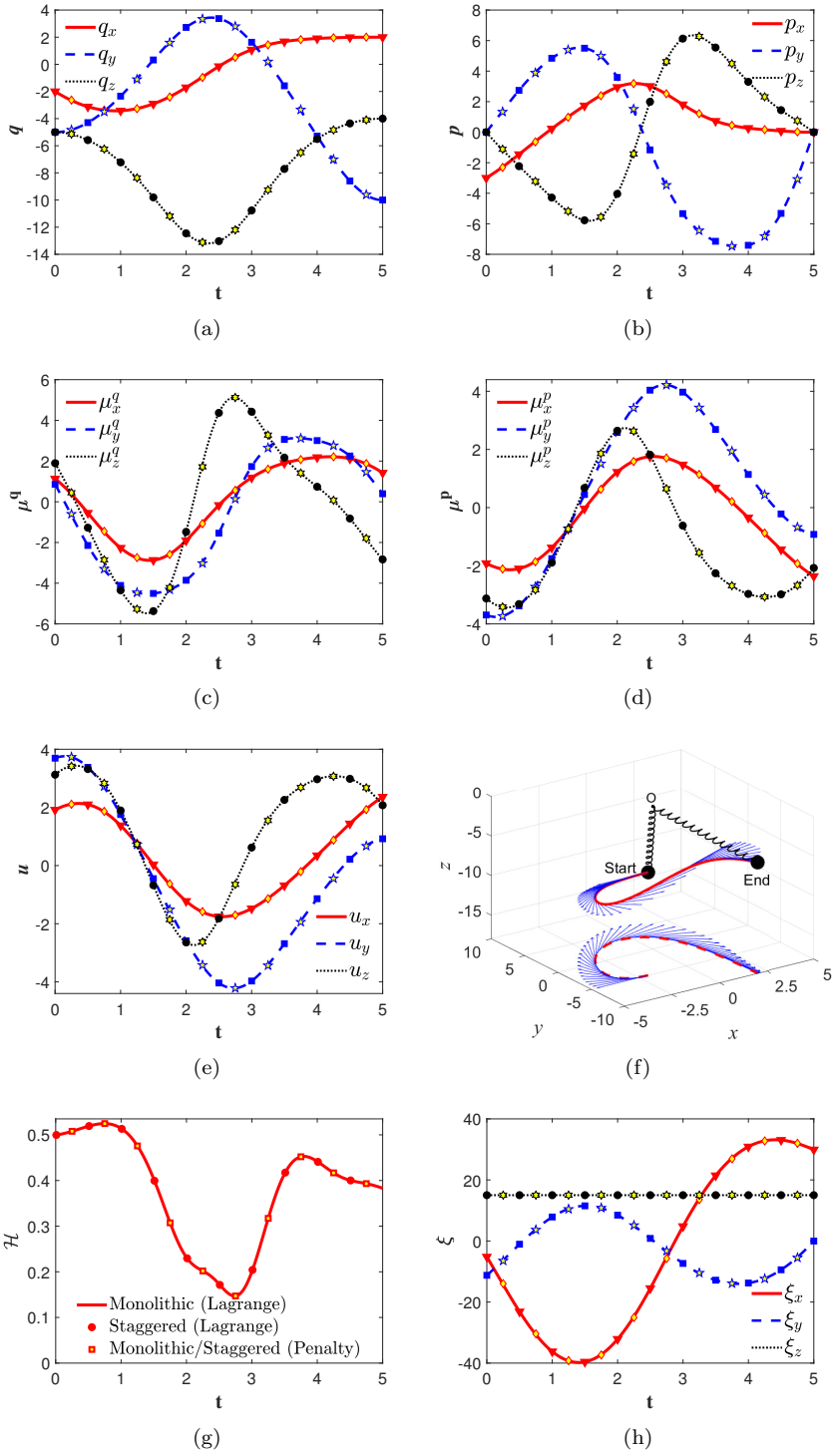

Figure 2: Minimal effort manoeuvring of 3D elastic pendulum (with Monolithic: $-$,$--$, $\cdots$, and FBSM-Newton: $\triangleright, \square, \circ$): (a,b) state (c,d) adjoint, (e) control, and (f) manoeuvring path in space and projected motion on x-y plane (arrow indicating the direction of momentum $\boldsymbol{p}$) (g) control Hamiltonian and (h) control angular momentum (Penalty: $\Diamond, \star, *$).

performance of the iterative solver is evident. Thus, one can conclude that the proposed hybrid strategy enhances the performance of both solvers by reducing the computational costs.

Table 2: 3D elastic pendulum: Comparison of solution strategies.

		Individual strategies				**Hybrid strategies**			
Problem size		**Monolithic**		**FBSM-Newton**		**FBSM-BB + Monolithic**		**FBSM-BB + FBSM-Newton**	
Δt(s)	DOF	Iter	CPU(s)	Iter	CPU(s)	Iter	CPU(s)	Iter	CPU(s)
0.5	165	7	2.57	9	2.25	25+6	2.24	25+6	2.07
0.1	765	9	56.29	9	34.08	25+6	35.78	25+6	25.68
0.05	1515	11	250.67	9	111.58	25+6	136.95	25+6	84.44
0.01	7515	15	8080.22	15	4516.84	25+6	3251.7	25+6	2010.23

6.2 3D rigid pendulum

An interesting and fundamental example to study the optimal control of constrained mechanical systems is a particle whose motion is confined to the surface of a sphere. Physically, this example may be viewed as a simplified version of an industrial robotic arm. Suppose the robot is working in a confined space and the shoulder is allowed to rotate freely without translation and the task is to find a control that moves the elbow with minimal effort from an initial position to the desired position in a given amount of time. To set up the problem, consider a particle with mass m, moving without friction on the surface of a sphere of radius l_o, and let $\boldsymbol{q} = (q_x, q_y, q_z) \in \mathcal{Q} = \mathbb{R}^3$ represent the position of the particle with respect to a Cartesian coordinate system fixed at the centre of the sphere (equipped with orthonormal right-handed basis vectors $\boldsymbol{E}_x, \boldsymbol{E}_y, \boldsymbol{E}_z$). Since we use more coordinates (redundant coordinates) than the actual degrees of freedom, additionally a holonomic constraint $\Phi(\boldsymbol{q}) = \frac{1}{2}(\boldsymbol{q} \cdot \boldsymbol{q} - l_o^2) = 0$ is imposed on the motion to ensure that the particle stays on the surface of the sphere. Correspondingly, the configuration manifold of the pendulum essentially is $\mathcal{S}^2 = \{\boldsymbol{q} \in \mathcal{Q} : \Phi(\boldsymbol{q}) = 0\} \subset \mathbb{R}^3$ (see Figure 4 b). The gravitational potential energy of the particle is $\mathcal{V}(\boldsymbol{q}) = ma\,\boldsymbol{q} \cdot \boldsymbol{E}_z$, where a is the acceleration due to gravity. It is important to note that the mechanical system is SO(3) invariant about the z-axis. The equations of motion correspond to those in (1), with control force $\boldsymbol{u} \in \mathbb{R}^3$, acting on the particle, and the augmented Hamiltonian $\mathcal{E}(\boldsymbol{q}, \boldsymbol{p}, \lambda) = \frac{1}{2m}\boldsymbol{p} \cdot \boldsymbol{p} + \mathcal{V}(\boldsymbol{q}) + \lambda\Phi(\boldsymbol{q})$, with $\lambda \in \mathbb{R}$ an unknown multiplier.

Now we phrase the optimal steering problem: find a control signal $\boldsymbol{u}(t)$ which steers the particle with minimal effort from the initial state $\boldsymbol{y}(0) = \overline{\boldsymbol{y}}_0$ to the desired final state $\boldsymbol{y}(T) = \boldsymbol{y}_d$ in prescribed time T. The cost functional $\mathcal{J}(\boldsymbol{y}, \boldsymbol{u})$ is again given by Eq (7).

To benchmark the results with different means to enforce the prescribed terminal state $\boldsymbol{y}(T) = \boldsymbol{y}_d$, we consider both the Lagrange type OCP ($\alpha = 1, \gamma = 1, \beta = 0, \beta_T = 0$) and the penalty type OCP ($\alpha = 10^{-3}, \gamma = 0, \beta = 0, \beta_T = 1$). It can be easily verified that the control Hamiltonian is autonomous and thus constitutes a conserved quantity (cf. Proposition 1). Furthermore, the control Hamiltonian is invariant with respect to rotations about gravity axis $\boldsymbol{E}_z$. Consequently, the control angular momentum about the z-axis, $\xi_z = \boldsymbol{E}_z \cdot (\boldsymbol{q} \times \boldsymbol{\mu}^q + \boldsymbol{p} \times \boldsymbol{\mu}^p)$, is a conserved quantity (cf. Proposition 2). Additionally, manoeuvring in free space (zero gravity) should result in the preservation of all three components of the control angular momentum.

In the numerical simulations we use the following data taken from [5]: $T = 1$, $l_o = 5$, $m = 1$, $a = 9.81$, $\overline{\boldsymbol{y}}_0 = (l_o, 0, 0, 0, 10, 0)$, $\boldsymbol{y}_d = (0, 0, -l_o, 0, 0, 0)$. Furthermore, we choose $\Delta t = 0.01$. We solve the optimal control problem by applying both the monolithic solver and FBSM. To initialize the problem, we choose an initial guess $\boldsymbol{u}(t) = (0, -2, 0)$ for $t \in [0, T]$, followed by solving the forward dynamics problem to populate the admissible phase space coordinates. In addition to that, we intentionally have chosen an initial momentum along the y-direction ($p_y = 10$), which enables the 3D motions and tends to move the particle away from the manifold (in the absence of holonomic constraints) and thus adds further difficulties to the numerical solution of the problem.

Note that using spherical coordinates (minimal coordinate representation) to describe the motion of the pendulum would introduce a singularity in the bottom-most position of the pendulum, unless a specific re-parametrisation of angles is applied, and thus would impede the imposition of the terminal state $\boldsymbol{y}(T) = \boldsymbol{y}_d$. Thus using redundant coordinates makes the present OCP much easier to handle.

Applying the Lagrange type OCP ($\alpha = 1, \gamma = 1, \beta = 0, \beta_T = 0$), we take into account Remark 3 to impose the terminal state $\boldsymbol{y}(T) = \boldsymbol{y}_d$. In particular, we use the null space matrix

$$\mathbf{P}(\boldsymbol{q}) = \frac{-1}{\sqrt{q_x^2 + q_z^2}} \begin{bmatrix} -q_z & q_x q_y / l_o \\ 0 & (q_y^2 - l_o^2)/l_o \\ q_x & q_y q_z / l_o \end{bmatrix}. \tag{46}$$

which automatically satisfies nullity $\nabla_{\boldsymbol{q}}\Phi(\boldsymbol{q})^{\mathsf{T}}\mathbf{P}(\boldsymbol{q}) = \mathbf{0}$, and orthonormality $\mathbf{P}(\boldsymbol{q})^{\mathsf{T}}\mathbf{P}(\boldsymbol{q}) = \mathbf{I}$. For similar applications of the null-space projections in optimal control problems and resorting to similar

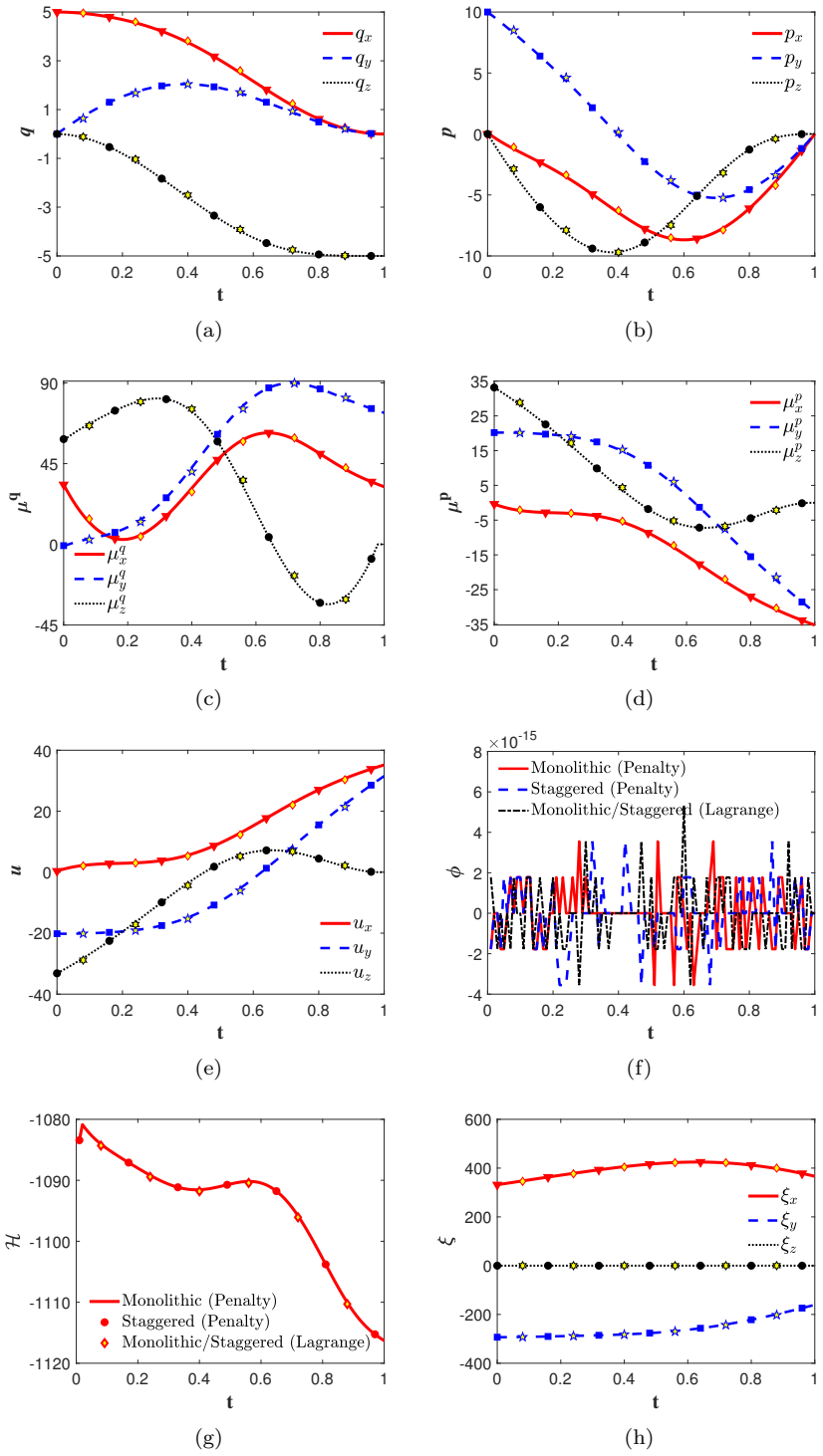

Figure 3: Minimal effort manoeuvring of a 3D rigid pendulum (with Monolithic: $-$,$--$, $\cdots$, and FBSM-Newton: $\triangleright, \square, \circ$): (a,b) state (c,d) adjoint, (e) control, and (f) holonomic constraint violation, (g) control Hamiltonian and (h) control angular momentum (Lagrange: $\Diamond, \star, *$).

FBSM solver, but with different temporal discretisation of the control equations, the reader may for instance refer to [41].

Applying the alternative penalty approach for the imposition of the terminal state $\boldsymbol{y}(T) = \boldsymbol{y}_d$, we use the penalty type OCP with $(\alpha = 10^{-3}, \gamma = 0, \beta = 0, \beta_T = 1)$. As can be seen from Figure 3, both penalty and Lagrange OCP solutions are in close agreement. As expected, the z-component of

Table 3: 3D rigid pendulum: Convergence of monolithic solver and FBSM-Newton ($\Delta t = 0.01$).

	Monolithic		**FBSM-Newton**	
Iteration	$\|\Delta \boldsymbol{w}\|_2$	$\|\boldsymbol{r}_w\|_2$	$\|\Delta \boldsymbol{\omega}\|_2$	$\|\boldsymbol{r}_u\|_2$
1	$4.310758e+01$	$1.495236e-01$	$2.114917e+01$	$2.818483e-02$
3	$5.303904e-05$	$2.262833e-12$	$2.371533e-01$	$8.877569e-06$
4	$5.505714e-11$	$7.811857e-13$	$4.291247e-03$	$2.661242e-09$
5			$9.920731e-08$	$5.282123e-14$
6			$1.936632e-11$	$3.431016e-14$

the control angular momentum is constant during manoeuvring. In addition to that, the holonomic constraint is satisfied up to machine accuracy which indicates that the particle stays on the correct configuration manifold (Figure 3 (f), see also the manoeuvring path in Figure 4). As discussed in Section 3.2, in the case *free space* ($a = 0$), all components of the control angular momentum are preserved, and as depicted in Figure 4 our numerical simulation corroborates this fact. Thus, we conclude that the SE1 scheme preserves the symplectic structure during numerical flow. Certainly, algorithmic preservation of the control Hamiltonian doesn't hold, see Figure 3 (g), due to the choice of the SE1 discretisation. However, the more the step-size is refined, the closer the control Hamiltonian comes to the constant value.

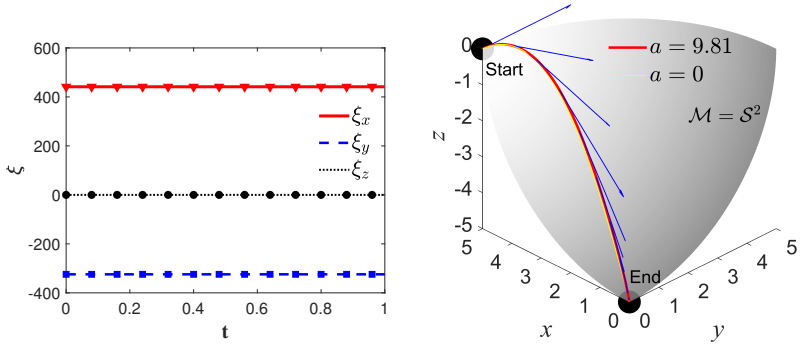

(a) (b)

Figure 4: Minimal effort manoeuvring of 3D rigid pendulum in free space (with Monolithic: $-$,$--$, $\cdots$, and FBSM-Newton: $\triangleright, \square, \circ$): (a) control angular momentum, and (b) manoeuvring path (in gravity and free space, equipped with the arrow indicating the direction of momentum $\boldsymbol{p}$).

Note that yet another viable choice of parameters for the penalty type OCP is given by $\alpha = 1, \gamma = 1, \beta = 0, \beta_T = 10^{-3}$. This choice does not require a special treatment to impose the terminal state $\boldsymbol{y}(T) = \boldsymbol{y}_d$ and yields numerical results close to those shown in Figure 3.

Finally, we study the robustness of the two solvers at our disposal, and the hybrid solution strategies. To this end, we increase the size of the NLP by decreasing the time step Δt, as shown in the first column of Table 4. We solve both problems (i.e. the penalty type OCP and the Lagrange type OCP) with both the monolithic and the staggered FBSM by using the same initial guess as described above (Table 3 indicates the convergence rate for Hybrid solvers). Although $\boldsymbol{u}(t) = (0, -2, 0)$ is indeed a very naive initial guess, the monolithic solver converges in 7 or 8 iterations, while the staggered FBSM-Newton requires many more iterations (see the second column in Table 4). Next, we utilise our hybrid solution strategies (see the third column in Table 4). Accordingly, it turns out that the slow convergence of FBSM-Newton is due to the bad quality of the initial guess. Again, the hybrid solvers are based on a 2-step procedure. We first apply the gradient descent solver FBSM-BB (stabilised Barzilai-Borwein line search, $\theta_{max} = 1$) with the same initial guess and, after 500 iterations, we invoke the Newton-based solvers, Monolithic or FBSM-Newton. As expected, the hybrid solution strategy improves the convergence behaviour of both, monolithic solver and FBSM-Newton (third and fourth columns in Table 4). Although the monolithic solver doesn't benefit from the hybrid solution strategy for small-size NLP, for moderately large size (for instance 1703 DOF) there is an insignificant difference in solution time compared with the individual Monolithic strategy. This suggests that a hybrid strategy has a clear advantage when the size of the NLP is sufficiently large.

Table 4: 3D rigid pendulum: Comparison of solution strategies.

		Individual strategies				**Hybrid strategies**			
Problem size		**Monolithic**		**FBSM-Newton**		**FBSM-BB + Monolithic**		**FBSM-BB + FBSM-Newton**	
Δt(s)	DOF	Iter	CPU(s)	Iter	CPU(s)	Iter	CPU(s)	Iter	CPU(s)
0.25	71	8	0.37	115	6.03	500+2	4.09	500+2	3.84
0.1	173	8	1.44	44	7	387+1	4.71	387+1	5.41
0.05	343	8	4.16	30	13.12	500+2	11.12	500+2	12.00
0.01	1703	7	82.94	30	261.73	500+4	88.98	500+6	94.11

Gradient-descent solver FBSM-BB already converged in 387 iterations, making FBSM-Newton solver convergence in just 1 iteration.

6.3 Swing-up of an inverted 2D pendulum. Rigid and elastic cases.

6.3.1 Rigid case

In this example, we study the control laws to stabilise a perturbed planar inverted rigid pendulum system. Inverted pendulum systems are often used to study and design the control laws for bipedal humanoid robots. Let the pair (q_1, q_2) and (q_3, q_4) denote the position of a cart (mass m_1) and a bob (mass m_2) in x-z plane, respectively (Figure 5). The current distance l between bob and cart results from $l(\boldsymbol{q})^2 = (q_3 - q_1)^2 + (q_4 - q_2)^2$. Since the cart is confined to move on a frictionless straight rail (x-axis), the configuration vector $\boldsymbol{q} = (q_1, q_3, q_4) \in \mathbb{R}^3$ fully describes the configuration of the present system.

Since the bob and the cart are connected by a rigid massless rod of length l_o, the system is subject to the holonomic constraint $\Phi(\boldsymbol{q}) = \frac{1}{2}(l(\boldsymbol{q})^2 - l_o^2) = 0$. Then the motion of the inverted rigid pendulum can be characterised by the translation q_1 of the base point, followed by a rotation of the rod with angle $\varphi = \tan^{-1}\left(\frac{q_4}{q_3 - q_1}\right)$. Thus, the configuration space of the present system can be viewed as 2-dimensional manifold (a cylindrical surface parametrised by q_1 and φ) embedded in $\mathcal{Q} = \mathbb{R}^3$. In other words, the configuration space is given by $\mathcal{M} = \mathbb{R} \times \mathbb{S}^1 = \{\boldsymbol{q} \in \mathcal{Q} : \Phi(\boldsymbol{q}) = 0\} \subset \mathbb{R}^3$ (see Figure 7 a). The gravitational potential energy of the system is defined as $\mathcal{V}(\boldsymbol{q}) = \boldsymbol{q} \cdot \mathbf{M}\boldsymbol{a}$ where $\mathbf{M} = \mathrm{diag}(m_1, m_2, m_2)$ is the mass matrix and $\boldsymbol{a} = (0, 0, a)$ is a gravitation field acting along the z-direction with intensity a. The equations of motion of the inverted rigid pendulum system fit into representation (1) with $\mathcal{E}(\boldsymbol{q}, \boldsymbol{p}, \lambda) = \frac{1}{2}\boldsymbol{p} \cdot \mathbf{M}^{-1}\boldsymbol{p} + \mathcal{V}(\boldsymbol{q}) + \lambda\Phi(\boldsymbol{q})$, $\lambda \in \mathbb{R}$ a Lagrange multiplier, and control force $\boldsymbol{u} = (u, 0, 0) \in \mathbb{R}^3$ such that the horizontal force $u \in \mathbb{R}$ is acting on the cart. Since the number of control inputs is less than the number of degrees of freedom, this example belongs to the important class of under-actuated mechanical control systems and indeed gives rise to a challenging optimal control problem.

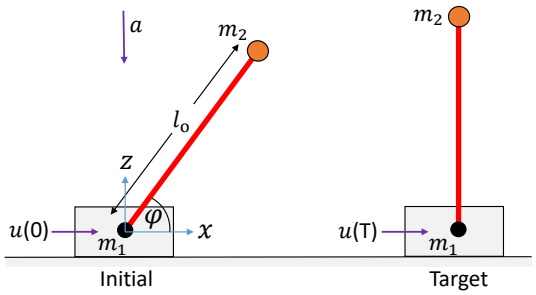

Figure 5: Inverted rigid pendulum: initial and desired configuration.

Now we are ready to formulate the optimal control problem: starting with an initial configuration $\boldsymbol{y}_0$, find a control signal $u(t)$ acting on the cart, which stabilises the pendulum about a vertical target configuration $\boldsymbol{y}_d$ (see Figure 5), within a given amount of time T. To achieve this goal we consider the objective functional Eq (7) with running cost similar to Eq (10). That is,

$$\mathcal{J}(\boldsymbol{y}, \boldsymbol{u}) = \int_0^T \mathcal{L}(\boldsymbol{y}, \boldsymbol{u}) dt \tag{47}$$

where $\mathcal{L}(\boldsymbol{y}, \boldsymbol{u}) = \frac{\beta}{2}(\boldsymbol{y} - \boldsymbol{y}_d)^\mathsf{T}\mathbf{Q}(\boldsymbol{y} - \boldsymbol{y}_d) + \frac{\alpha}{2}\boldsymbol{u}^\mathsf{T}\boldsymbol{u}$ is a tracking type running cost, and $\alpha, \beta \in \mathbb{R}^+$. Note

that the control Hamiltonian, $\mathcal{H}(\boldsymbol{y},\boldsymbol{u};\boldsymbol{\mu}) = \mathcal{L}(\boldsymbol{y},\boldsymbol{u}) + \boldsymbol{\mu}\cdot\boldsymbol{f}(\boldsymbol{y},\boldsymbol{u},\lambda) + \zeta\Phi(\boldsymbol{q})$, is the only constant of motion of the posed OCP.

In the numerical simulations we use the following data: $\Delta t = 0.01$, $T = 2$, $m_1 = 2$, $m_2 = 0.2$, $a = 1$, $\beta = 1$, $\alpha = 10^{-4}$, $\overline{\boldsymbol{y}}_0 = (0, 0.5, 1, 0, 0, 0)$, $\boldsymbol{y}_d = (0, 0, 2, 0, 0, 0)$, $\mathbf{Q} = \mathrm{diag}(0, 0, 1, 0, 0, 0)$. Moreover, we provide a naive initial guess for the control input given by $u(t) = 1$ for $t \in [0, T]$. Admissible initial states are generated by solving the forward dynamics problem.

We first study the convergence of both monolithic solver and FBSM-Newton. From Table 5, one can infer that the staggered FBSM-Newton converges quadratically and yields the optimal solution in fewer iterations than the monolithic solver. Moreover, both solvers predict similar optimal solutions (see Figure 6). Due to the inclined initial position of the pendulum, a large force needs to be applied initially to swing up and then gradually retard to keep the pendulum in an upright position (see Figure 6 b and e). Figure 7 (a-f) shows the variation of rod inclination angle φ and 7 a the horizontal position q_1 of the cart, which affirms that indeed the optimal configuration trajectory evolves over the cylindrical surface with q_1, the axial coordinate and φ, the polar angle . Once the system gets stabilised the control force almost vanishes and the linear momentum attains a steady state value. Additionally, to keep the system in a stabilised configuration, the synchronous horizontal motion of the cart and the bob is essential and can be verified from state trajectories (Figure 6 a and b). Moreover, since we have no terminal cost in this example, the adjoint variables $\boldsymbol{\mu}$ should vanish at the final time (Figure 6 c and d).

Table 5: 2D rigid pendulum: Convergence of monolithic solver and FBSM-Newton ($\Delta t = 0.01$).

	Monolithic		**FBSM-Newton**	
Iteration	$\|\Delta \boldsymbol{w}\|_2$	$\|\boldsymbol{r}_w\|_2$	$\|\Delta \boldsymbol{\omega}\|_2$	$\|\boldsymbol{r}_u\|_2$
1	$3.086121e+02$	$1.198159e+01$	$3.723607e+01$	$4.154488e-01$
4	$2.784208e+02$	$1.099290e+01$	$3.057142e+00$	$2.173781e-04$
5	$9.570851e+01$	$9.159894e+00$	$2.944943e-02$	$2.266004e-08$
6	$4.109482e+01$	$3.957286e+00$	$2.873218e-06$	$4.508789e-14$
7	$1.819356e+01$	$9.460896e-01$	$3.643147e-13$	$1.207341e-14$
12	$3.201166e-12$	$1.192913e-13$		

6.3.2 Elastic case

Next, we consider an elastic variant of the inverted pendulum system dealt with before. In particular, we deal with the stabilisation of an under-actuated elastic inverted pendulum system. Here bob and cart are connected by an elastic spring which allows the bob to move freely in the x-z plane. Concerning the changes to the previously treated inverted pendulum problem, we essentially replace the holonomic constraint $\Phi(\boldsymbol{q}) = 0$ with a nonlinear elastic spring, whose potential is given by

$$\mathcal{V}_e(\boldsymbol{q}) = \lambda\Phi(\boldsymbol{q})^2 = \frac{\lambda}{4}(l(\boldsymbol{q})^2 - l_o^2)^2$$

Consequently, the equations of motion now assume the form of ODEs instead of DAEs, and in the optimal control problem we now have to deal with OCP-ODE instead of OCP-DAE.

In the numerical simulations we choose $\lambda = 10$. Apart from this, we repeat the simulations in the framework of OCP-ODE without any changes to the data previously used in the framework of OCP-DAE. We again apply both the monolithic solver and FBSM-Newton.

The numerical results obtained with $\Delta t = 0.01$ are shown in Figure 8. Accordingly, the optimal solution of the swing-up manoeuvre is again characterised by a decaying control signal and a synchronous horizontal motion of the cart and the bob after the swing-up, similar to the case of the rigid pendulum. However, due to the presence of the elastic spring, and that *the height of the target position $\boldsymbol{y}_d$ is larger then the static equilibrium height of the spring $z_{eqm} = 1.099$, we can* observe longitudinal oscillations of the spring, which remain after the swing-up has taken place around a distance shorter than the initial length l_o (see Figure 8 a and b). We have verified that such oscillations indeed diminish when $\boldsymbol{y}_d = (0, 0, z_{eqm}, 0, 0, 0\}$, although they do not fully disappear. Similar oscillations can be observed in the adjoint variables (Figure 8 c and d). Moreover, the control Hamiltonian has some minor variations which is expected since SE1 is not capable to conserve the control Hamiltonian.

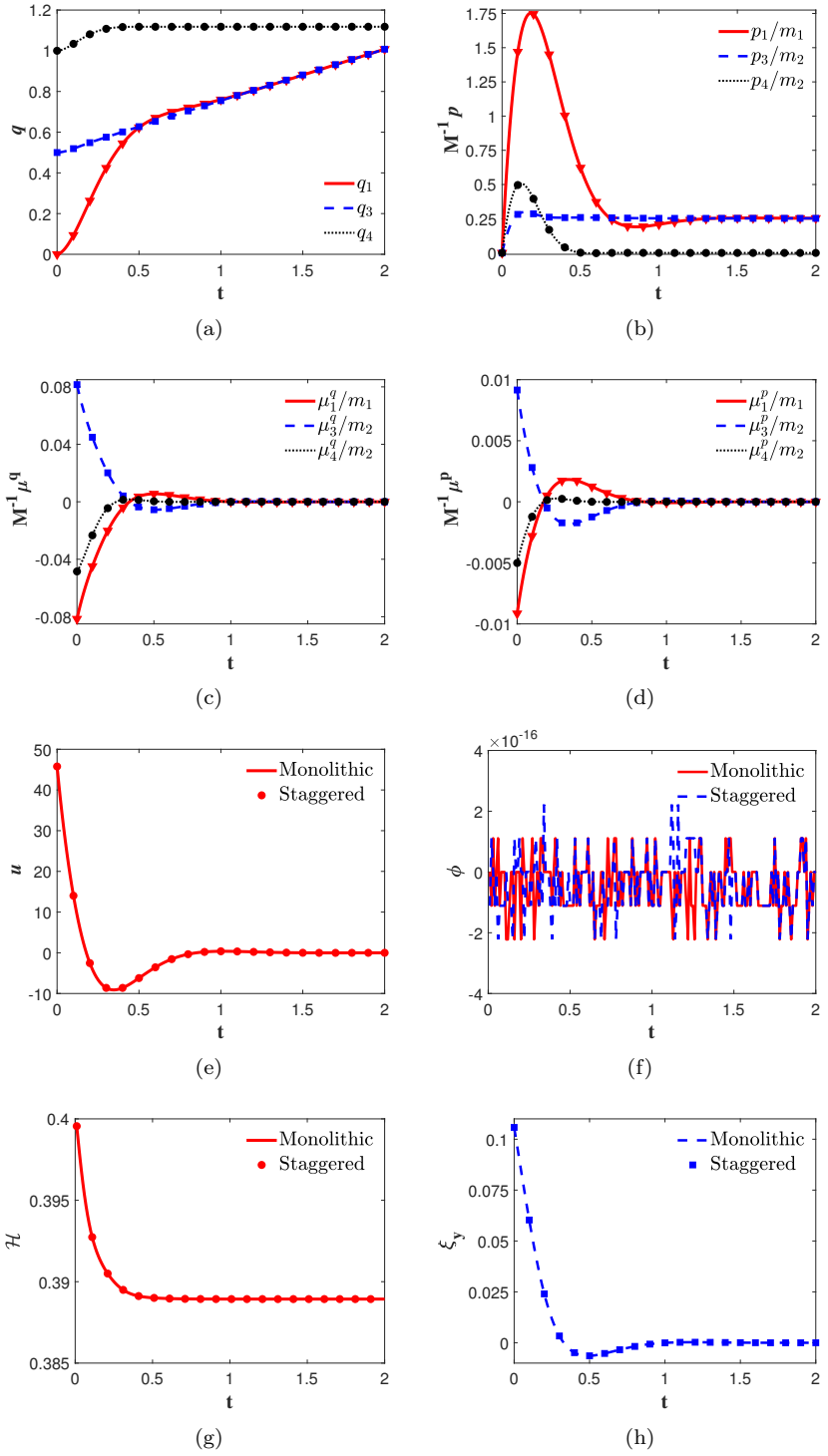

Figure 6: 2D rigid pendulum optimal trajectories (with Monolithic: $-$,$--$, $\cdots$, and FBSM-Newton: $\triangleright, \square, \circ$): (a,b) state (c,d) adjoint, (e) control force (with manoeuvring path), and (f) constraint violation (g) control Hamiltonian and (h) control angular momentum.

Finally, we conduct a study on the efficacy of monolithic solver and FBSM-Newton, and present a comparison with the hybrid solution strategies. To this end, we consider both the rigid and the elastic pendulum. Using the same initial guess as before, we increase the size of the NLP by decreasing Δt (first column in Tables 6 and 7).

One can observe from the second column in Tables 6 and 7 that the FBSM-Newton converges in less iterations and takes less computational time than the monolithic solver. This holds true for

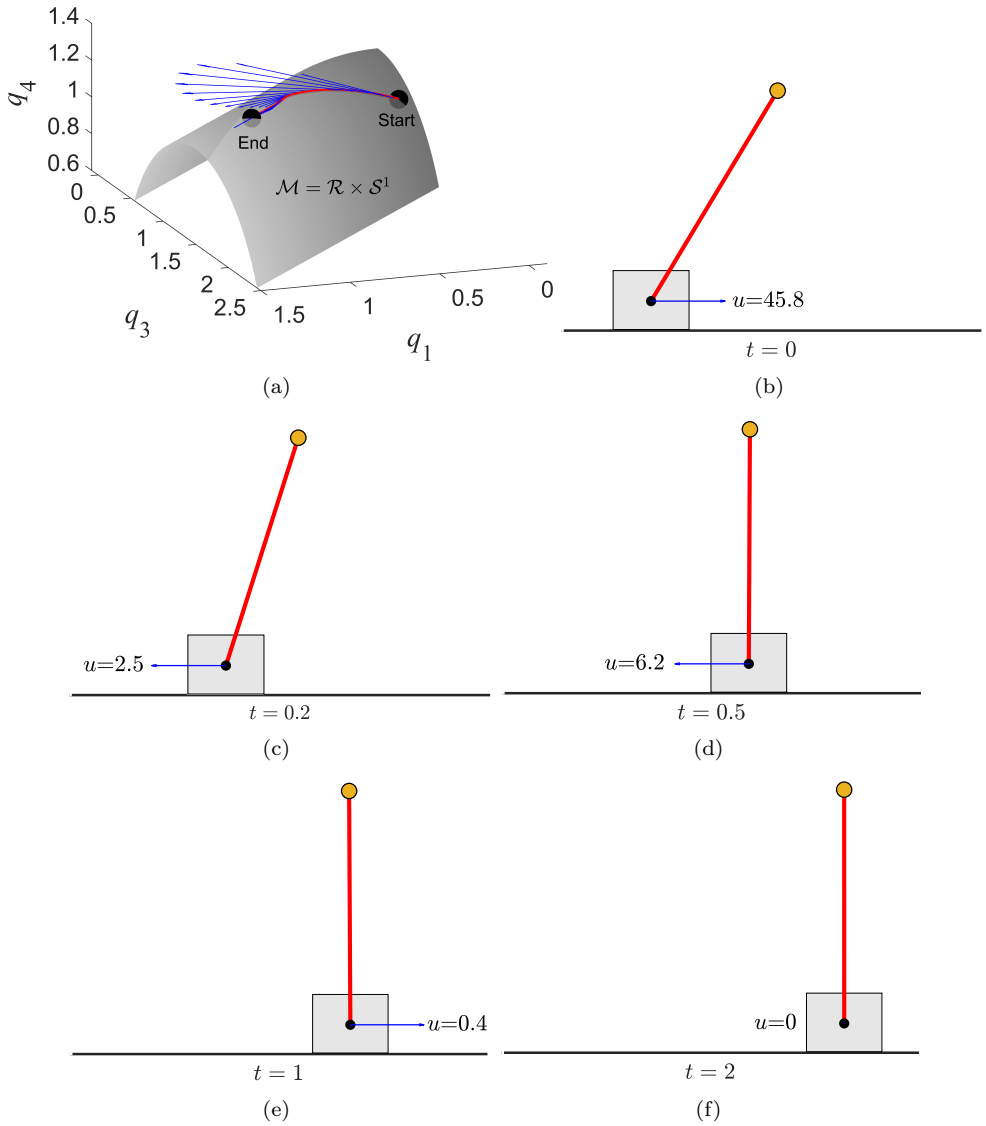

Figure 7: 2D rigid pendulum optimal control: (a) manoeuvring path over constraint manifold $\mathcal{M}$ (equipped with the arrow indicating the direction of velocity $\mathbf{M}^{-1}\boldsymbol{p}$), and (b-f) snapshot of the motion with control effort at times $t \in \{0, 0.2, 0.5, 1, 2\}$.

Table 6: 2D rigid pendulum: Comparison of solution strategies.

		Individual strategies				**Hybrid strategies**			
Problem size		**Monolithic**		**FBSM**		**FBSM-BB + Monolithic**		**FBSM-BB + FBSM-Newton**	
Δt(s)	DOF	Iter	CPU(s)	Iter	CPU(s)	Iter	CPU(s)	Iter	CPU(s)
0.1	301	13	8.90	7	1.67	25+7	5.03	25+9	2.61
0.05	601	13	33.64	7	4.95	25+8	19.49	25+8	6.41
0.01	3001	12	745.7	7	102.11	25+8	465.29	25+7	103.1
0.005	6001	13	3394.41	7	401.3	25+8	1881.25	25+7	390.21

both the rigid pendulum (Table 6) and the elastic pendulum (Table 7). Concerning the hybrid 2-step procedures, we perform the first 25 iterations with the standard gradient-based FBSM-BB (with a stabilised Barzilai-Borwein line search, $\theta_{max} = 1$) and then invoke either the monolithic solver or FBSM-Newton. As can be observed from the third column in Tables 6 and 7, the hybrid solution approaches significantly improve the convergence and reduce the solution time of the monolithic solver. However, the hybrid solution approaches yield only a marginal reduction in the computational

effort of the staggered FBSM-Newton.

Table 7: 2D elastic pendulum: Comparison of alternative solution strategies.

		Individual strategies				**Hybrid strategies**			
Problem size		**Monolithic**		**FBSM-Newton**		**FBSM-BB + Monolithic**		**FBSM-BB + FBSM-Newton**	
Δt(s)	DOF	Iter	CPU(s)	Iter	CPU(s)	Iter	CPU(s)	Iter	CPU(s)
0.1	261	14	9.48	9	1.93	25+6	4.94	25+9	2.57
0.05	521	14	36.33	7	4.67	25+6	16.98	25+10	8.13
0.01	2601	19	1190.3	8	138.9	25+8	502.42	25+9	135.22
0.005	5201	18	4708.65	8	450.85	25+8	2016.67	25+8	482.07

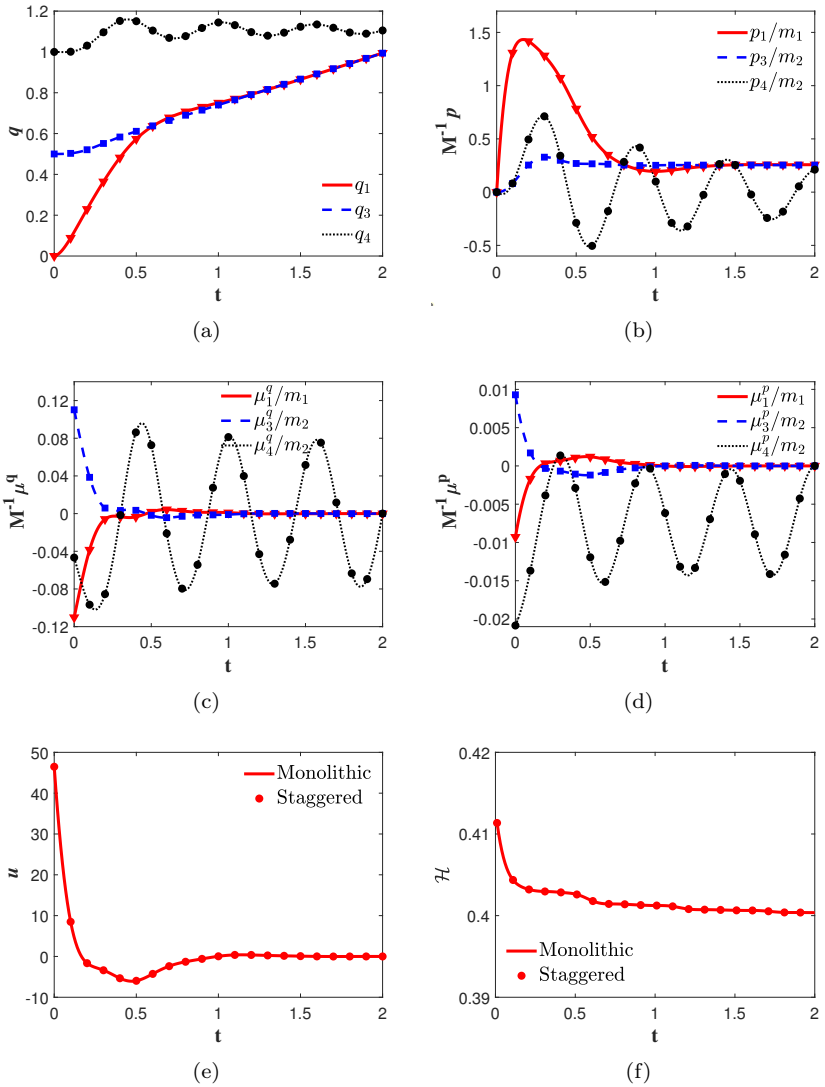

Figure 8: 2D elastic pendulum optimal trajectories (with Monolithic: $-$,$--$, $\cdots$, and FBSM-Newton: $\triangleright, \square, \circ$): time evolution of (a,b) state (c,d) adjoint, (e) control force (with manoeuvring path), and (f) control Hamiltonian.

7 Conclusions

We have presented alternative approaches to the solution of optimal control problems for constrained mechanical systems. Using redundant coordinates provides a general and versatile framework for the formulation of the equations of motion pertaining to controlled mechanical systems. Correspondingly, the state equations of the optimal control problem assume the form of index-3 differential-algebraic equations (DAEs). We presented a direct approach leading to discrete conditions of optimality that (i) ensure that the holonomic constraints of the underlying mechanical system are satisfied, and (ii) preserves the symplectic structure of the underlying Hamiltonian boundary value problem. Accordingly, the discrete state equations guarantee that the mechanical system stays on the correct configuration manifold. Moreover, the structure-preserving discretisation implies the conservation of control angular momentum maps which result from a rotational symmetry of the underlying optimal control problem.

The discrete optimality conditions give rise to a nonlinear programming problem (NLP) which can be solved in different ways. For that purpose we investigated two alternative solution approaches which both rely on the Newton-Raphson method and thus guarantee quadratic rates of convergence in the vicinity of the optimal trajectory. The first approach relies on the monolithic solution of the NLP and thus leads to a comparatively large algebraic system of equations which can be solved by the Newton-Raphson method in a straightforward way. The second approach, FBSM-Newton, is based on the Forward-Backward Sweep Method of the NLP that bears some similarities with the conventional gradient-based approach which also goes under the name (discrete) adjoint method [41]. Our newly proposed FBSM-Newton scheme introduces the following two crucial features. The introduction of auxiliary adjoint variables facilitates the treatment of prescribed end-point conditions for the state variables. Moreover, since the FBSM-Newton relies on the application of the Newton-Raphson method, it provides the aforementioned advantageous convergence properties. This is in sharp contrast to conventional gradient-based FBSM solvers which are typically plagued with an extremely slow converge behaviour in the vicinity of the optimal trajectory.

In addition to the two individual solvers, we presented two hybrid solution procedures which are based on a 2-step procedure. In the first step a conventional FBSM-BB gradient-based solver is applied with the goal to provide a good initial guess for the Newton-Raphson-based solvers that are applied in a second step.

Our numerical experiments show that the optimal trajectories obtained with both the monolithic solver and the FBSM-Newton are in close agreement. In addition to that, the hybrid solution strategies were shown to mitigate the convergence issue and reduce the computational effort. We also verified with numerical examples that the proposed SE1 discretisation method does indeed preserve the control angular momentum maps associated with rotational symmetries of the underlying optimal control problem. Concerning the treatment of prescribed final states we showed that both, the penalty type approach and the exact imposition by means of Lagrange multipliers, led to reliable results for both the monolithic solver and the FBSM-Newton.

We remark that in the type of problems presented and tested here, the objective function of the OCP was a quadratic function, and that the admissible set of the controls is unbounded. This is an ideal situation for the Hessian-based and line-search algorithms, as those tested here. Therefore, our conclusions may not carry over to non-smooth functionals or bounded control sets, unless more sophisticated strategies are incorporated.

The FBSM-Newton as well as the 2-step hybrid solution strategies appear to be especially well-suited to deal with large-scale optimal control problems. Large-scale state equations (DAEs or ODEs) may arise from the finite element discretisation of continuous mechanical problems such as beams or continuum bodies [10, 13]. In future work, the structure-preserving discretisation of optimal control problems may also address the conservation of the control Hamiltonian in addition to control momentum maps associated with symmetries of the optimal control problem.

8 Acknowledgments

This work is financially supported by the Spanish Ministry of Science and Innovation, under Severo Ochoa program CEX2018-000797-S, and the research project DynAd2, with reference PID2020-116141GB-I00. The financial support of the local government of Generalitat de Catalunya under grant 2021 SGR 01049 is also acknowledged. Further financial support has been provided by the Deutsche Forschungsgemeinschaft (DFG, German Research Foundation) – Projektnummer 442997215.

9 Conflict of interest

The authors declare no potential conflict of interests.

References

[1] Arnold VI. *Mathematical methods of classical mechanics*. Springer Science; 2013.

[2] Ascher UM, Petzold, LR. *Computer methods for ordinary differential equations and differential-algebraic equations*. Society for Industrial and Applied Mathematics (SIAM), 2nd edition; 1998.

[3] Barzilai J, Borwein, JM. Two-point step size gradient methods. *IMA Journal of Numerical Analysis* 1988; 8(1):141-148.

[4] Betsch P, Becker C. Conservation of generalized momentum maps in mechanical optimal control problems with symmetry. *Int. J. Num. Meth. Engng.* 2017; 111:144-155.

[5] P. Betsch and S. Schneider. Conservation of generalized momentum maps in the optimal control of constrained mechanical systems. *IFAC-PapersOnLine*, 54(9):615-9, 2021.

[6] Betsch P. The discrete null space method for the energy consistent integration of constrained mechanical systems: Part I: Holonomic constraints. *Comp. Meth. Appl. Mech. Engng.* 2005; 194(50-52):5159-90.

[7] Betsch P, Steinmann P. A DAE approach to flexible multibody dynamics. *Mult. Syst. Dyn.* 2002; 8:367-391.

[8] Betsch P, Siebert R, Sänger N. Natural coordinates in the optimal control of multibody systems. *J. Comput. Nonlinear Dynam.* 2012; 7(1):011009/1-8.

[9] Betts JT. *Practical Methods for Optimal Control and Estimation Using Nonlinear Programming*. Society for Industrial and Applied Mathematics (SIAM), Philadelphia, USA, 2nd edition; 2010.

[10] Bijalwan A. Numerical optimisation of worm locomotion on frictional substrates. *PhD Thesis. Universitat Politècnica de Catalunya.*URL: https://upcommons.upc.edu/handle/2117/415062, 2024.

[11] Bijalwan A, Muñoz JJ. A control Hamiltonian-preserving discretisation for optimal control. *Mult. Syst. Dyn.* 2023; 59:19–43.

[12] Bijalwan A, Muñoz JJ. On the numerical stability of discretised optimal control problems. *IUTAM Bookseries, vol 42. Springer*; 2024.

[13] Bijalwan A, Muñoz, JJ. Adjoint-based optimal control of contractile elastic bodies. Application to limbless locomotion on frictional substrates. *Comp. Meth. Appl. Mech. Engng.* 2024; 450:116697.

[14] Bloch AM, Bloch AM. *Nonholonomic Mechanics and Control*. Springer, New York; 2003.

[15] Bryson AE, Ho YC. *Applied Optimal Control. Optimization, Estimation and Control*. Taylor & Francis, New York, U.S.A.; 1975.

[16] Cantrijn F, de León M, Marrero JC, Martín de Diego D. Reduction of constrained systems with symmetries. *J. Math. Phys.* 1999; 40(2):795-820.

[17] Echeverría-Enríquez A, Marín-Solano J, Muñoz-Lecanda MC, Román-Roy N. Geometric reduction in optimal control theory with symmetries. *Rep. Math. Phys.* 2003; 52(1):89–113.

[18] Eichmeir P, Nachbagauer K, Lauß T, Sherif K, Steiner W. Time-optimal control of dynamic systems regarding final constraints. *J. Comput. Nonlinear Dynam.* 2021; 16(3):031003.

[19] Flaßkamp K, Murphey TD. Structure-preserving local optimal control of mechanical systems. *Optim. Control Appl. Methods* 2019; 40(2):310-329.

[20] Gear CW, Gupta GK, Leimkuhler B. Automatic integration of Euler-Lagrange Equations with Constraints. *J. Comput. Appl. Math.* 1985; 12-13:77-90.

[21] Gerdts M. *Optimal control of ODEs and DAEs.* Walter de Gruyter GmbH & Co KG; 2023.

[22] Gotay MJ, Nester JM Presymplectic lagrangian systems. I: The constraint algorithm and the equivalence theorem. *Annales de l'I.H.P. Phys. Théor.* 1979; 30:129-142.

[23] Hairer E, Lubich C, and Wanner G. *Geometric numerical integration: structure-preserving algorithms for ordinary differential equations.* Springer-Verlag; 2002.

[24] Holm DD. *Geometric mechanics-Part I: Dynamics and symmetry.* World Scientific Publishing Company; 2011.

[25] Lasdon LS, Mitter SK, Waren AD. The conjugate gradient method for optimal control problems. *IEEE Trans. Aut. Cont.* 1967; 12(2):132–138.

[26] Leyendecker S, Ober-Blöbaum S, Marsden JE, M. Ortiz. Discrete mechanics and optimal control for constrained multibody dynamics. *International Design Engineering Technical Conferences and Computers and Information in Engineering Conference* 2007; 4806:623-632.

[27] Leyendecker S, Ober-Blöbaum S, Marsden JE, Ortiz M. Discrete mechanics and optimal control for constrained systems. *Optim. Control Appl. Methods* 2010; 31(6):505-528.

[28] Leyendecker S, S Maslovskaya, Ober-Blöbaum S, de Almagro RTSM, Szemenyei FO A new Lagrangian approach to control affine systems with a quadratic Lagrange term. *J. Comp. Dyn.* 2024; 11(3):336-353.

[29] Lenhart S, Workman JT. *Optimal control applied to biological models.* Chapman and Hall/CRC; 2007.

[30] Marsden JE. *Lectures on mechanics.* Cambridge University Press, 1992.

[31] Muñoz JJ, Jelenič G. Sliding joints in 3D beams: conserving algorithms using the master–slave approach. *Mult. Syst. Dyn.* 2006; 16:237–261.

[32] Nachbagauer K, Oberpeilsteiner S, Sherif K, Steiner W. The use of the adjoint method for solving typical optimization problems in multibody dynamics. *J. Comput. Nonlinear Dynam.* 2015; 10(6).

[33] Nocedal J, Wright SJ. *Numerical Optimization.* Springer, New York, 2nd edition; 2006.

[34] Ober-Blöbaum S, Junge O, Marsden JE. Discrete mechanics and optimal control: An Analysis. *ESAIM: Cont. Opt. Cal. Var.* 2011; 17(2):322-352.

[35] Kinon PL, Betsch P, Schneider S. The GGL variational principle for constrained mechanical systems. *Mult. Syst. Dyn.* 2023; 57(3-4):211–236.

[36] Kinon PL, Betsch P, Schneider S. Structure-preserving integrators based on a new variational principle for constrained mechanical systems. *Nonlin. Dyn.* 2023; 111(15):14231–14261.

[37] Roubíček T, Valášek M. Optimal control of causal differential–algebraic systems. *J. Math. Anal. Appl.* 2002; 269(2):616-41.

[38] Sanz-Serna JM. Symplectic Runge-Kutta schemes for adjoint equations, automatic differentiation, optimal control, and More. *SIAM Review* 2016; 58(1):3-33.

[39] Schneider S,Betsch P. On optimal control problems in redundant coordinates. *Proceedings of the 11th ECCOMAS Thematic Conference on Multibody Dynamics.* 2023.

[40] Schneider S, Betsch P. Optimal control of constrained mechanical systems in redundant coordinates: Formulation and structure-preserving discretization. *Comp. Meth. Appl. Mech. Engng.* 2024; 432(1):117443.

[41] Schubert M, Sato Martín de Almagro RT, Nachbagauer K, Ober-Blöbaum S, Leyendecke S. Discrete adjoint method for variational integration of constrained ODEs and its application to optimal control of geometrically exact beam dynamics. *Mult. Syst. Dyn.* 2024; 60 (3):447-474.

[42] Simo JC, Tarnow N, Wong K. Exact energy-momentum conserving algorithms and symplectic schemes for nonlinear dynamics. *Comp. Meth. Appl. Mech. Engng.* 1992; 100(1):63-116.

[43] Tran BK, Leok M. Geometric methods for adjoint systems. *J. Nonlin. Sc.* 2024; 34(1):25.

[44] Van der Schaft AJ. Symmetries in optimal control. *SIAM J. Cont. Opt.* 1987; 25(2):245-259.

[45] Wang Y, Ranner T, Ilett TP, Xia Y, Cohen N. A monolithic optimal control method for displacement tracking of cosserat rod with application to reconstruction of *C. elegans* locomotion. *Comput. Mech.* 2023; 71(3):409-432.

[46] Wijckmans PMEJ. *Differential algebraic equations.* RANA: reports on applied and numerical analysis, Eindhoven University of Technology, 1992.

10 Supporting information

Additional supporting information may be found in the online version of the article at the publisher's website.

A Proof of symplecticity of optimal control problem

The symplecticity of the Hamiltonian differential equation $\dot{\boldsymbol{z}} = \mathbb{J}\nabla\mathcal{H}(\boldsymbol{z})$ is well established. However, in optimal control problems, the dependence of the Hamiltonian function $\mathcal{H}$ on a control function $\boldsymbol{u}(t)$, which also depends on $\boldsymbol{z}(t)$ makes this symplectic structure less clear. We here show that sympleciticity is retained in optimal control problems in the absence of holonomic constraints, that is for the equations in (13) with $\boldsymbol{s} = \boldsymbol{u}$.

Proposition 4. *If components $\boldsymbol{y}$ in variable $\boldsymbol{z} = (\boldsymbol{y}, \boldsymbol{\mu})$ form a set of minimal coordinates, the Hamiltonian $\mathcal{H}(\boldsymbol{z}, \boldsymbol{u})$ is at least twice differentiable, and $\nabla_{uu}\mathcal{H}$ is non degenerated, then the constrained ODE in* (13) *in the absence of holonomic constraints is symplectic in the sense that, for any optimal control $\boldsymbol{u}(\boldsymbol{z})$, the Hamiltonian flow $\boldsymbol{z}(t) = \boldsymbol{\varphi}_t(\boldsymbol{z}_0, \boldsymbol{u}(\boldsymbol{z}))$ of the solution satisfies the condition $\mathbf{A}^T\mathbb{J}\mathbf{A} = \mathbb{J}$ with $\mathbf{A} = \frac{\partial \boldsymbol{\varphi}}{\partial \boldsymbol{z}_0}$.*

Proof. The constraint $\nabla_u \mathcal{H} = \mathbf{0}$ furnishes a relation $\boldsymbol{u}(\boldsymbol{z})$ that, for a regular functional $\mathcal{H}(\boldsymbol{z}, \boldsymbol{u})$, and from the implicit function theorem, satisfies

$$\mathbf{Z} := \frac{\partial \boldsymbol{u}}{\partial \boldsymbol{z}} = -\left(\nabla^2_{uu}\mathcal{H}\right)^{-1} \nabla^2_{uz}\mathcal{H}. \tag{48}$$

Consequently, the ODE in (13) provides a map $\bar{\boldsymbol{z}} = \varphi_t(\boldsymbol{z}, \boldsymbol{u}(\boldsymbol{z}))$, where the time derivative of the Jacobian $\mathbf{A} = \frac{\partial \boldsymbol{z}}{\partial \boldsymbol{z}_0}$ reads,

$$\frac{d}{dt}\mathbf{A} = \frac{d}{d\boldsymbol{z}}\mathbb{J}\nabla_z\mathcal{H}\mathbf{A} = \mathbb{J}\left(\frac{\partial \nabla_z \mathcal{H}}{\partial \boldsymbol{u}}\mathbf{Z} + \frac{\partial \nabla_z \mathcal{H}}{\partial \boldsymbol{z}}\right)\mathbf{A} = \mathbb{J}\left(\nabla^2_{zu}\mathcal{H}\mathbf{Z} + \nabla^2_{zz}\mathcal{H}\right)\mathbf{A}$$

For $t = 0$, we have that $\mathbf{A} = \mathbf{I}$, and thus clearly $\mathbf{A}^T\mathbb{J}\mathbf{A} = \mathbb{J}$. For $t > 0$, we have from the previous result and relations $\mathbb{J}^T = \mathbb{J}^{-1} = -\mathbb{J}$ and $\mathbb{J}^2 = -\mathbb{I}$,

$$\frac{d}{dt}\left(\mathbf{A}^T\mathbb{J}\mathbf{A}\right) = \mathbf{A}^T\left(\left(\nabla^2_{zu}\mathcal{H}\mathbf{Z} + \nabla^2_{zz}\mathcal{H}\right)^T - \left(\nabla^2_{zu}\mathcal{H}\mathbf{Z} + \nabla^2_{zz}\mathcal{H}\right)\right)\mathbf{A}$$

which vanishes due to expression of $\mathbf{Z}$ in (48), symmetry of $\nabla^2_{uu}\mathcal{H}$ and regularity of $\mathcal{H}$, i.e. $\nabla^2_{uz}\mathcal{H} = \nabla^2_{zu}\mathcal{H}^T$. □

In the presence of the constraints, the Hessian $\nabla_{ss}\mathcal{H}$ is singular, and thus the result above cannot be applied for this case, unless a null-space projection of the constraints is employed, and thus the equations are rewritten in terms of minimal coordinates.

B Symplectic integrator for Hamiltonian boundary value problem

The optimality conditions expressed in terms of differential $(\boldsymbol{y}, \boldsymbol{\mu})$ and algebraic variable $\boldsymbol{s}$ reads

$$\begin{aligned}
\dot{\boldsymbol{y}} &= \nabla_{\boldsymbol{\mu}}\mathcal{H}(\boldsymbol{y}, \boldsymbol{\mu}, \boldsymbol{s}) \\
\dot{\boldsymbol{\mu}} &= -\nabla_{\boldsymbol{y}}\mathcal{H}(\boldsymbol{y}, \boldsymbol{\mu}, \boldsymbol{s}) \\
\mathbf{0} &= \nabla_{\boldsymbol{s}}\mathcal{H}(\boldsymbol{y}, \boldsymbol{\mu}, \boldsymbol{s}).
\end{aligned} \tag{49}$$

We here consider general $\tau-$ integration schemes for Hamiltonian boundary value problem (HBVP) (see Eq (13)), where the state and adjoint variables in the gradients above are evaluated at different time points, as discussed in [4, 13]. As we will show next, only a few choices of τ retain the symplecticity of the numerical flow.

Proposition 5. *Partitioned Euler scheme with $(\tau_y, \tau_\mu) = \left((0,1), (\frac{1}{2}, \frac{1}{2}), (1,0)\right)$ is a symplectic integrator for the autonomous constrained mechanical control system:*

$$\begin{aligned}
\boldsymbol{y}_n - \boldsymbol{y}_{n-1} &= \Delta t \nabla_{\boldsymbol{\mu}}\mathcal{H}(\boldsymbol{y}_{n-1+\tau_y}, \boldsymbol{\mu}_{n-1+\tau_\mu}, \boldsymbol{s}_{(\cdot)}) \\
\boldsymbol{\mu}_n - \boldsymbol{\mu}_{n-1} &= -\Delta t \nabla_{\boldsymbol{y}}\mathcal{H}(\boldsymbol{y}_{n-1+\tau_y}, \boldsymbol{\mu}_{n-1+\tau_\mu}, \boldsymbol{s}_{(\cdot)}) \\
\mathbf{0} &= \nabla_{\boldsymbol{s}}\mathcal{H}(\boldsymbol{y}_{n+\tau_y-1}, \boldsymbol{\mu}_{n-1+\tau_\mu}, \boldsymbol{s}_{(\cdot)}).
\end{aligned}$$

with $(\bullet)_{n-1+\tau} := (1-\tau)(\bullet)_{n-1} + \tau(\bullet)_n$.

Proof. Time discretisation of DAE TPBVP with symplectic Euler scheme reads ($\tau_y, \tau_\mu \in \{0, 1\}$)

$$\boldsymbol{r}(\boldsymbol{y}_{n-1}, \boldsymbol{\mu}_{n-1}; \boldsymbol{y}_n, \boldsymbol{\mu}_n; \boldsymbol{s}_{(\cdot)}) = \begin{bmatrix} \boldsymbol{y}_n - \boldsymbol{y}_{n-1} - \Delta t \nabla_{\boldsymbol{\mu}}\mathcal{H}(\boldsymbol{y}_{n-1+\tau_y}, \boldsymbol{\mu}_{n-1+\tau_\mu}, \boldsymbol{s}_{(\cdot)}) \\ \boldsymbol{\mu}_n - \boldsymbol{\mu}_{n-1} + \Delta t \nabla_{\boldsymbol{y}}\mathcal{H}(\boldsymbol{y}_{n-1+\tau_y}, \boldsymbol{\mu}_{n-1+\tau_\mu}, \boldsymbol{s}_{(\cdot)}) \end{bmatrix} = \mathbf{0} \tag{50}$$

Consider the flow of numerical scheme $f : \boldsymbol{z}_{n-1} \to \boldsymbol{z}_n$ with Jacobian $\mathbf{F}$, where phase vector $\boldsymbol{z}_{n-1} := \{\boldsymbol{y}_{n-1}, \boldsymbol{\mu}_{n-1}\}$ and $\boldsymbol{z}_n := \{\boldsymbol{y}_n, \boldsymbol{\mu}_n\}$ represents the numerical state at current (t_n) and previous time (t_{n-1}), respectively. The discretisation scheme in which new state perturbation/increments ($\delta \boldsymbol{z}_n$) are the symplectic transformation of the previous state perturbation/increments ($\delta \boldsymbol{z}_{n-1}$) is known as symplectic algorithm, i.e., $\delta \boldsymbol{z}_n = \mathbf{F}\delta \boldsymbol{z}_{n-1}$ [42]. Suppose the algebraic variables and underneath

algebraic constraints are consistently discretised with some $\tau_s \in [0,1]$, and we perturb differential flow variable ($\boldsymbol{z}$) at time t_{n-1} and t_n. Linearising residue about ($\boldsymbol{z}_n$, $\boldsymbol{z}_{n-1}$), we obtain

$$\boldsymbol{r}\left(\boldsymbol{z}_n + \delta\boldsymbol{z}_n, \boldsymbol{z}_{n-1} + \delta\boldsymbol{z}_{n-1}\right) = \boldsymbol{r}\left(\boldsymbol{z}_n, \boldsymbol{z}_{n-1}\right) + \frac{\partial \boldsymbol{r}}{\partial \boldsymbol{z}_n}\delta\boldsymbol{z}_n + \frac{\partial \boldsymbol{r}}{\partial \boldsymbol{z}_{n-1}}\delta\boldsymbol{z}_{n-1} = \boldsymbol{0} \tag{51}$$

With Eq. (50) and transformation $\delta\boldsymbol{z}_n = \mathbf{F}\delta\boldsymbol{z}_{n-1}$, Jacobian of the map can be written as

$$\mathbf{F} = \left(\frac{\partial \boldsymbol{r}}{\partial \boldsymbol{z}_n}\right)^{-1}\left(-\frac{\partial \boldsymbol{r}}{\partial \boldsymbol{z}_{n-1}}\right) \tag{52}$$

If we define $\mathbf{F} := \mathbf{B}^{-1}\mathbf{C}$, then for symplectic transformation

$$\mathbf{F}^{\mathsf{T}}\mathbb{J}\mathbf{F} = \mathbb{J} \Leftrightarrow \mathbf{B}\mathbb{J}\mathbf{B}^{\mathsf{T}} - \mathbf{C}\mathbb{J}\mathbf{C}^{\mathsf{T}} = \mathbf{0} \tag{53}$$

For partitioned Euler discretisation, $\mathbf{B}$ and $\mathbf{C}$ matrices reads ($\mathbf{K} := \nabla_{\boldsymbol{y}}(\nabla_{\boldsymbol{\mu}}\mathcal{H})$)

$$\mathbf{B} = \begin{bmatrix} \mathbb{I} - \tau_y\Delta t\mathbf{K} & \mathbb{O} \\ \tau_y\Delta t\nabla_{\boldsymbol{y}}(\nabla_{\boldsymbol{y}}\mathcal{H}) & \mathbb{I} + \tau_\mu\Delta t\mathbf{K}^T \end{bmatrix}, \quad \mathbf{C} = \begin{bmatrix} \mathbb{I} + (1-\tau_y)\Delta t\mathbf{K} & \mathbb{O} \\ -(1-\tau_y)\Delta t\nabla_{\boldsymbol{y}}(\nabla_{\boldsymbol{y}}\mathcal{H}) & \mathbb{I} - (1-\tau_\mu)\Delta t\mathbf{K}^T \end{bmatrix}$$

One can deduce the following expressions

$$\mathbf{B}\mathbb{J}\mathbf{B}^{\mathsf{T}} = \begin{bmatrix} \mathbb{O} & \mathbb{I} + (\tau_\mu - \tau_y)\Delta t\mathbf{K} - \tau_\mu\tau_y\Delta t^2\mathbf{K}\mathbf{K} \\ -\mathbb{I} - (\tau_\mu - \tau_y)\Delta t\mathbf{K}^T + \tau_\mu\tau_y\Delta t^2\mathbf{K}^T\mathbf{K}^T & \mathbb{O} \end{bmatrix}$$

$$\mathbf{C}\mathbb{J}\mathbf{C}^{\mathsf{T}} = \begin{bmatrix} \mathbb{O} & \mathbb{I} + (\tau_\mu - \tau_y)\Delta t\mathbf{K} - (1-\tau_\mu)(1-\tau_y)\Delta t^2\mathbf{K}\mathbf{K} \\ -\mathbb{I} - (\tau_\mu - \tau_y)\Delta t\mathbf{K}^T + (1-\tau_\mu)(1-\tau_y)\Delta t^2\mathbf{K}^T\mathbf{K}^T & \mathbb{O} \end{bmatrix}$$

If one chooses the combination $(\tau_y, \tau_\mu) = \{(0,1), (\frac{1}{2}, \frac{1}{2}), (1,0)\}$, coupling terms vanish and we obtain $\mathbf{B}\mathbb{J}\mathbf{B}^{\mathsf{T}} = \mathbf{C}\mathbb{J}\mathbf{C}^{\mathsf{T}}$. Which affirms that $\mathbf{F}^{\mathsf{T}}\mathbb{J}\mathbf{F} = \mathbb{J}$ and $\mathbf{F}$ is a symplectic transformation and the above three choices form a symplectic integrator for a constrained mechanical control system.

□

Among three choices of symplectic integrator viz SE1($\tau_y = 1, \tau_\mu = 0$), SE2($\tau_y = 0, \tau_\mu = 1$), and Mid-Point rule (SMP)($\tau_y = \tau_\mu = \frac{1}{2}$), SE2 results in an explicit scheme for forward and backward integration of state-adjoint system (conditionally stable) and not suitable while attempting iterative solution of NLP (see Box 1). Although SMP is a second-order scheme with nice convergence properties [4, 11], it introduces numerical oscillation in optimal trajectories with diminishing α. Alternatively, the SE1 has twofold advantages first it forms an implicit scheme (unconditionally stable) for forward and backward integration of the state-adjoint system, and second, it provides additional stability against numerical oscillations for diminishing α or large Δt [12]. Considering this SE2 and SMP has been discarded and SE1 integrator has been used in all numerical examples with $\tau_y = \tau_\lambda = 1, \tau_\mu = \tau_\zeta = \tau_u = 0$. Since SE1 is a first-order scheme, preservation of control Hamiltonian at local and global levels uphold only up to $\mathcal{H}_n - \mathcal{H}_{n-1} \sim \mathcal{O}(\Delta t^2)$, and $\mathcal{H}_n - \mathcal{H}_0 \sim \mathcal{O}(\Delta t)$, respectively [23]. As expected, by virtue of its symplectic property preserves discrete momentum-maps corresponding to rotational symmetry and upholds up to the machine's accuracy.

C Necessary conditions for direct approach

We will here proof that the direct approach and the indirect approach yield the same NLP for SE1 algorithm. For this, we resort to a generic time integration scheme with the notation $\boldsymbol{y}_{n-1+\tau} := (1-\tau)\boldsymbol{y}_{n-1} + \tau\boldsymbol{y}_n, \tau \in [0,1]$, and write the following minimisation problem:

$$\begin{aligned} &\min_{\mathbf{y},\mathbf{u}} \mathcal{J}_\Delta(\mathbf{y}, \mathbf{u}) \\ &\text{s.t., } \boldsymbol{y}_n - \boldsymbol{y}_{n-1} = \boldsymbol{f}_\Delta(\boldsymbol{y}_{n-1}, \boldsymbol{y}_n, \boldsymbol{\lambda}_n, \boldsymbol{u}_{n-1}) \\ &\qquad \boldsymbol{\Phi}_\Delta(\boldsymbol{y}_{n-1}, \boldsymbol{y}_n) = \boldsymbol{0} \\ &\qquad \gamma\mathbf{g}_T(\boldsymbol{y}_N) = \boldsymbol{0} \\ &\qquad \boldsymbol{y}_0 - \bar{\boldsymbol{y}}_0 = \boldsymbol{0} \end{aligned}$$

with the following definitions of the discrete functions:

$$\begin{aligned} \boldsymbol{f}_\Delta(\boldsymbol{y}_{n-1}, \boldsymbol{y}_n, \boldsymbol{\lambda}_n, \boldsymbol{u}_{n-1}) &:= \Delta t\boldsymbol{f}(\boldsymbol{y}_{n-1+\tau}, \boldsymbol{u}_{n-1}) \\ \boldsymbol{\Phi}_\Delta(\boldsymbol{y}_{n-1}, \boldsymbol{y}_n) &:= \Delta t\boldsymbol{\Phi}_q(\boldsymbol{y}_{n-1+\tau}) \\ \mathcal{L}_\Delta(\boldsymbol{y}_{n-1}, \boldsymbol{y}_n, \boldsymbol{u}_{n-1}) &:= \Delta t\mathcal{L}(\boldsymbol{y}_{n-1+\tau}, \boldsymbol{u}_{n-1}) \\ \mathcal{J}_\Delta(\mathbf{y}, \mathbf{u}) &:= \beta_T\psi(\boldsymbol{y}_N) + \sum_{n=1}^{N}\mathcal{L}_\Delta(\boldsymbol{y}_{n-1}, \boldsymbol{y}_n, \boldsymbol{u}_{n-1}) \end{aligned}$$

Next, we introduce the adjoint variables $\boldsymbol{\mu} = \{\mu_0, \ldots, \boldsymbol{\mu}_N\}$, $\boldsymbol{\zeta} = \{\boldsymbol{\zeta}_0, \ldots, \boldsymbol{\zeta}_{N-1}\}$ and $\boldsymbol{\eta}$, along with auxiliary state $\boldsymbol{b} = \{\boldsymbol{b}_0, \ldots, \boldsymbol{b}_{N-1}\}$ and adjoint $\boldsymbol{\rho} = \{\boldsymbol{\rho}_0, \ldots, \boldsymbol{\rho}_{N-1}\}$. These auxiliary variable will play a key role in deducing the algorithmic preservation of the momentum map. From them, we build the associated discrete Hamiltonian $\mathcal{H}_\Delta$ of the direct approach as

$$\mathcal{H}_\Delta(\boldsymbol{y}_{n-1}, \boldsymbol{b}_{n-1}, \boldsymbol{\lambda}_n, \boldsymbol{u}_{n-1}; \boldsymbol{\mu}_n, \boldsymbol{\rho}_{n-1}, \boldsymbol{\zeta}_{n-1}) = \mathcal{L}_\Delta(\boldsymbol{y}_{n-1}, \boldsymbol{b}_{n-1}, \boldsymbol{u}_{n-1}) + (\boldsymbol{\rho}_{n-1} + \boldsymbol{\mu}_n)^\mathsf{T} \boldsymbol{f}_\Delta(\boldsymbol{y}_{n-1}, \boldsymbol{b}_{n-1}, \boldsymbol{\lambda}_n, \boldsymbol{u}_{n-1}) + \boldsymbol{\zeta}_{n-1}^\mathsf{T} \boldsymbol{\Phi}_\Delta(\boldsymbol{y}_{n-1}, \boldsymbol{b}_{n-1} \tag{54}$$

and the corresponding discrete Lagrangian functional $\mathcal{S}_\Delta$, rewritten as

$$\begin{aligned}\mathcal{S}_\Delta(\cdot) = &\sum_{n=1}^{N} \Big[\mathcal{H}_\Delta(\boldsymbol{y}_{n-1}, \boldsymbol{b}_{n-1}, \boldsymbol{\lambda}_n, \boldsymbol{u}_{n-1}; \boldsymbol{\mu}_n, \boldsymbol{\rho}_{n-1}, \boldsymbol{\zeta}_{n-1}) + (\boldsymbol{\mu}_n + \boldsymbol{\rho}_{n-1})^\mathsf{T} \boldsymbol{y}_{n-1} - \boldsymbol{\mu}_n^\mathsf{T} \boldsymbol{y}_n - \boldsymbol{\rho}_{n-1}^\mathsf{T} \boldsymbol{b}_{n-1}\Big] \\ &+ \beta_T \psi(\boldsymbol{y}_N) + \gamma \boldsymbol{\eta}^\mathsf{T} \boldsymbol{g}_T(\boldsymbol{y}_N) - \boldsymbol{\mu}_0^\mathsf{T}(\boldsymbol{y}_0 - \overline{\boldsymbol{y}}_0).\end{aligned} \tag{55}$$

Then, the first-variation of discrete Lagrangian $\mathcal{S}_\Delta$ reads

$$\begin{aligned}\delta\mathcal{S}_\Delta(\cdot) = &\sum_{n=1}^{N} \left(\nabla_{\boldsymbol{y}_{n-1}} \mathcal{H}_\Delta + \boldsymbol{\mu}_n - \boldsymbol{\mu}_{n-1} + \boldsymbol{\rho}_{n-1}\right) \cdot \delta \boldsymbol{y}_{n-1} + \sum_{n=1}^{N} \left(\nabla_{\boldsymbol{b}_{n-1}} \mathcal{H}_\Delta - \boldsymbol{\rho}_{n-1}\right) \cdot \delta \boldsymbol{b}_{n-1} \\ &+ \sum_{n=1}^{N} \left(\nabla_{\boldsymbol{\mu}_n} \mathcal{H}_\Delta - \boldsymbol{y}_n + \boldsymbol{y}_{n-1}\right) \cdot \delta \boldsymbol{\mu}_n + \sum_{n=1}^{N} \left(\nabla_{\boldsymbol{\rho}_{n-1}} \mathcal{H}_\Delta - \boldsymbol{b}_{n-1} + \boldsymbol{y}_{n-1}\right) \cdot \delta \boldsymbol{\rho}_{n-1} \\ &+ \sum_{n=1}^{N} \left(\nabla_{\boldsymbol{\lambda}_n} \mathcal{H}_\Delta\right) \cdot \delta \boldsymbol{\lambda}_n + \sum_{n=1}^{N} \left(\nabla_{\boldsymbol{u}_{n-1}} \mathcal{H}_\Delta\right) \cdot \delta \boldsymbol{u}_{n-1} + \sum_{n=1}^{N} \left(\nabla_{\boldsymbol{\zeta}_{n-1}} \mathcal{H}_\Delta\right) \cdot \delta \boldsymbol{\zeta}_{n-1} \\ &+ \Big(\beta_T \nabla_{\boldsymbol{y}_N} \psi(\boldsymbol{y}_N) + \gamma \nabla_{\boldsymbol{y}_N} \boldsymbol{g}_T(\boldsymbol{y}_N)^\mathsf{T} \boldsymbol{\eta} - \boldsymbol{\mu}_N\Big) \cdot \delta \boldsymbol{y}_N + \gamma \boldsymbol{g}_T(\boldsymbol{y}_N) \cdot \delta \boldsymbol{\eta} - (\boldsymbol{y}_0 - \overline{\boldsymbol{y}}_0) \cdot \delta \boldsymbol{\mu}_0.\end{aligned}$$

and the stationarity of Lagrangian functional (KKT conditions) furnishes the following NLP ($n = 1, \cdots, N$)

$$\boldsymbol{\mu}_n - \boldsymbol{\mu}_{n-1} = -\nabla_{\boldsymbol{y}_{n-1}} \mathcal{H}_\Delta - \boldsymbol{\rho}_{n-1} \tag{56a}$$
$$\boldsymbol{\rho}_{n-1} = \nabla_{\boldsymbol{b}_{n-1}} \mathcal{H}_\Delta \tag{56b}$$
$$\boldsymbol{y}_n - \boldsymbol{y}_{n-1} = \nabla_{\boldsymbol{\mu}_n} \mathcal{H}_\Delta \tag{56c}$$
$$\boldsymbol{b}_{n-1} - \boldsymbol{y}_{n-1} = \nabla_{\boldsymbol{\rho}_{n-1}} \mathcal{H}_\Delta \tag{56d}$$
$$\boldsymbol{0} = \nabla_{\boldsymbol{\lambda}_n} \mathcal{H}_\Delta \tag{56e}$$
$$\boldsymbol{0} = \nabla_{\boldsymbol{\zeta}_{n-1}} \mathcal{H}_\Delta \tag{56f}$$
$$\boldsymbol{0} = \nabla_{\boldsymbol{u}_{n-1}} \mathcal{H}_\Delta \tag{56g}$$
$$\boldsymbol{0} = \gamma \boldsymbol{g}_T(\boldsymbol{y}_N) \tag{56h}$$
$$\boldsymbol{0} = \beta_T \nabla_{\boldsymbol{y}_N} \psi(\boldsymbol{y}_N) + \gamma \nabla_{\boldsymbol{y}_N} \boldsymbol{g}_T(\boldsymbol{y}_N)^\mathsf{T} \boldsymbol{\eta} - \boldsymbol{\mu}_N \tag{56i}$$
$$\boldsymbol{0} = \boldsymbol{y}_0 - \overline{\boldsymbol{y}}_0. \tag{56j}$$

Using the fact $\nabla_{\boldsymbol{\mu}_n} \mathcal{H}_\Delta = \nabla_{\boldsymbol{\rho}_{n-1}} \mathcal{H}_\Delta = \boldsymbol{f}_\Delta$ and compare Eq (56c) and Eq (56d), we conclude $\boldsymbol{b}_{n-1} = \boldsymbol{y}_n$. Next, we make use of Eq (18) to calculate the gradient of discrete Hamiltonian function. For evaluation point $(\boldsymbol{y}_{(n-1+\tau)}, \boldsymbol{\lambda}_n, \boldsymbol{u}_{n-1}, \boldsymbol{\mu}_n, \boldsymbol{\rho}_{n-1}, \boldsymbol{\zeta}_{n-1})$, right hand side of Eq (56a) and (56b) reduces to

$$\begin{aligned}\nabla_{\boldsymbol{y}_{n-1}} \mathcal{H}_\Delta &= (1-\tau)\Delta t \nabla_{\boldsymbol{y}} \mathcal{H}(\boldsymbol{y}_{n-1+\tau}, \boldsymbol{\lambda}_n, \boldsymbol{u}_{n-1}; \boldsymbol{\mu}_n + \boldsymbol{\rho}_{n-1}, \boldsymbol{\zeta}_{n-1}) \\ \nabla_{\boldsymbol{b}_{n-1}} \mathcal{H}_\Delta &= \tau \Delta t \nabla_{\boldsymbol{y}} \mathcal{H}(\boldsymbol{y}_{n-1+\tau}, \boldsymbol{\lambda}_n, \boldsymbol{u}_{n-1}; \boldsymbol{\mu}_n + \boldsymbol{\rho}_{n-1}, \boldsymbol{\zeta}_{n-1}).\end{aligned} \tag{57}$$

Substituting Eq (57) into Eq (56a) and (56b) and compare both equations, we obtain

$$\boldsymbol{\mu}_n - \boldsymbol{\mu}_{n-1} + \boldsymbol{\rho}_{n-1} = -\frac{(1-\tau)}{\tau} \boldsymbol{\rho}_{n-1} \Rightarrow \boldsymbol{\rho}_{n-1} = -\tau(\boldsymbol{\mu}_n - \boldsymbol{\mu}_{n-1}), \tag{58}$$

Additionally, using this relation, we define (here $\tau_\mu = 1 - \tau$)

$$\boldsymbol{\mu}_{n-1+\tau_\mu} := \boldsymbol{\mu}_n + \boldsymbol{\rho}_{n-1} = (1-\tau_\mu)\boldsymbol{\mu}_{n-1} + \tau_\mu \boldsymbol{\mu}_n. \tag{59}$$

Using Eq (58), and Eq (59), discrete Hamiltonian function can be expressed as

$$\mathcal{H}_\Delta = \Delta t \mathcal{H}(\boldsymbol{y}_{n-1+\tau}, \boldsymbol{\lambda}_n, \boldsymbol{u}_{n-1}; \boldsymbol{\mu}_{n-1+\tau_\mu}, \boldsymbol{\zeta}_{n-1}). \tag{60}$$

Thus choice $\tau = 1$ gives the evaluation point $(\boldsymbol{y}_n, \boldsymbol{\lambda}_n, \boldsymbol{u}_{n-1}, \boldsymbol{\mu}_{n-1}, \boldsymbol{\zeta}_{n-1})$, and utilising Eq (60), we obtain the same NLP shown in Box 1. The next propositions also shows that this choice also preserves the control angular momentum.

Proposition 6. *If the discrete control Hamiltonian $\mathcal{H}_\Delta$ in* (54) *is invariant of superimposed rigid rotation about an axis whose direction given by a unit vector $\boldsymbol{n}$, then the numerical flow induced by NLP in* (56a)-(56g) *conserves the control angular momentum in a sense that $\boldsymbol{\xi}_n \cdot \boldsymbol{n} = \boldsymbol{\xi}_{n-1} \cdot \boldsymbol{n}$. where*

$$\boldsymbol{\xi}_{(\bullet)} := \boldsymbol{y}_{(\bullet)} \star \boldsymbol{\mu}_{(\bullet)} = \sum_{i=1}^{n} \boldsymbol{q}^i_{(\bullet)} \times (\boldsymbol{\mu}^q_{(\bullet)})^i + \boldsymbol{p}^i_{(\bullet)} \times (\boldsymbol{\mu}^p_{(\bullet)})^i \tag{61}$$

Proof. The infinitesimal change in the discrete control Hamiltonian under the superimposed rigid rotation $(\boldsymbol{y}_{n-1}, \boldsymbol{b}_{n-1}, \boldsymbol{u}_{n-1}) \to (\boldsymbol{y}_{n-1} + d\boldsymbol{y}_{n-1}, \boldsymbol{b}_{n-1} + d\boldsymbol{b}_{n-1}, \boldsymbol{u}_{n-1} + d\boldsymbol{u}_{n-1})$ and $(\boldsymbol{\mu}_{n-1}, \boldsymbol{\rho}_{n-1}) \to (\boldsymbol{\mu}_{n-1} + d\boldsymbol{\mu}_{n-1}, \boldsymbol{\rho}_{n-1} + d\boldsymbol{\rho}_{n-1})$ about $\boldsymbol{n}$, such that $d(\bullet)^i = \varepsilon(\boldsymbol{n} \times (\bullet)^i)$ yields

$$\begin{aligned}
&\frac{d}{d\varepsilon}\mathcal{H}_\Delta(\boldsymbol{y}_{n-1} + d\boldsymbol{y}_{n-1}, \boldsymbol{b}_{n-1} + d\boldsymbol{b}_{n-1}, \boldsymbol{\lambda}_n, \boldsymbol{u}_{n-1} + d\boldsymbol{u}_{n-1}, \boldsymbol{\mu}_n + d\boldsymbol{\mu}_n, \boldsymbol{\rho}_{n-1} + d\boldsymbol{\rho}_{n-1}, \boldsymbol{\zeta}_{n-1})\Big|_{\varepsilon=0} \\
&= \nabla_{\boldsymbol{y}_{n-1}}\mathcal{H}_\Delta \cdot \hat{\boldsymbol{y}}_{n-1} + \nabla_{\boldsymbol{b}_{n-1}}\mathcal{H}_\Delta \cdot \hat{\boldsymbol{b}}_{n-1} + \nabla_{\boldsymbol{\mu}_{n-1}}\mathcal{H}_\Delta \cdot \hat{\boldsymbol{\mu}}_{n-1} + \nabla_{\boldsymbol{\rho}_{n-1}}\mathcal{H}_\Delta \cdot \hat{\boldsymbol{\rho}}_{n-1} + \nabla_{\boldsymbol{u}_{n-1}}\mathcal{H}_\Delta \cdot \hat{\boldsymbol{u}}_{n-1}
\end{aligned}$$

where hat denotes $\hat{(\bullet)}^i_{n-1} = \boldsymbol{n} \times (\bullet)^i_{n-1}$.

If the discrete control Hamiltonian remains invariant under this transformation, terms on the right hand-side of the above expression vanish. Substituting Eq (56a)-(56d) and Eq (56g) into the above expression yields

$$(-\boldsymbol{\mu}_n + \boldsymbol{\mu}_{n-1} - \boldsymbol{\rho}_{n-1}) \cdot \hat{\boldsymbol{y}}_{n-1} + \boldsymbol{\rho}_{n-1} \cdot \hat{\boldsymbol{b}}_{n-1} + (\boldsymbol{y}_n - \boldsymbol{y}_{n-1}) \cdot \hat{\boldsymbol{\mu}}_n + (\boldsymbol{b}_{n-1} - \boldsymbol{y}_{n-1}) \cdot \hat{\boldsymbol{\rho}}_{n-1} = 0$$

Rearrangement of the above expression results in

$$\begin{aligned}
-(\boldsymbol{\mu}_n \cdot \hat{\boldsymbol{y}}_{n-1} + \boldsymbol{y}_{n-1} \cdot \hat{\boldsymbol{\mu}}_n) - (\boldsymbol{\rho}_{n-1} \cdot \hat{\boldsymbol{y}}_{n-1} + \boldsymbol{y}_{n-1} \cdot \hat{\boldsymbol{\rho}}_{n-1}) + (\boldsymbol{\rho}_{n-1} \cdot \hat{\boldsymbol{b}}_{n-1} + \boldsymbol{b}_{n-1} \cdot \hat{\boldsymbol{\rho}}_{n-1}) \\
+ \boldsymbol{\mu}_{n-1} \cdot \hat{\boldsymbol{y}}_{n-1} + \boldsymbol{y}_n \cdot \hat{\boldsymbol{\mu}}_n = 0
\end{aligned} \tag{62}$$

where terms in the parentheses cancel out due to the property of vector triple product, i.e., $\boldsymbol{a} \cdot (\boldsymbol{n} \times \boldsymbol{b}) + \boldsymbol{b} \cdot (\boldsymbol{n} \times \boldsymbol{a}) = 0$, for $(\boldsymbol{a}, \boldsymbol{b}, \boldsymbol{n}) \in \mathbb{R}^3$. For instance:

$$\begin{aligned}
(\boldsymbol{\mu}_n \cdot \hat{\boldsymbol{y}}_{n-1} + \boldsymbol{y}_{n-1} \cdot \hat{\boldsymbol{\mu}}_n) = &\sum_{i=1}^{n} (\boldsymbol{\mu}^q_n)^i \cdot (\boldsymbol{n} \times \boldsymbol{q}^i_{n-1}) + (\boldsymbol{\mu}^p_n)^i \cdot (\boldsymbol{n} \times \boldsymbol{p}^i_{n-1}) \\
&+ \sum_{i=1}^{n} \boldsymbol{q}^i_{n-1} \cdot (\boldsymbol{n} \times (\boldsymbol{\mu}^q_n)^i) + \boldsymbol{p}^i_{n-1} \cdot (\boldsymbol{n} \times (\boldsymbol{\mu}^p_n)^i) = 0.
\end{aligned}$$

Therefore, using the property of the vector triple product and the $\star$ product, the expression in Eq (62) simplifies to

$$\boldsymbol{\mu}_{n-1} \cdot \hat{\boldsymbol{y}}_{n-1} + \boldsymbol{y}_n \cdot \hat{\boldsymbol{\mu}}_n = \boldsymbol{n} \cdot (\boldsymbol{y}_{n-1} \star \boldsymbol{\mu}_{n-1}) - \boldsymbol{n} \cdot (\boldsymbol{y}_n \star \boldsymbol{\mu}_n) = \boldsymbol{\xi}_{n-1} \cdot \boldsymbol{n} - \boldsymbol{\xi}_n \cdot \boldsymbol{n} = 0$$

and the preservation of the control angular momentum follows

$$\boldsymbol{\xi}_n \cdot \boldsymbol{n} = \boldsymbol{\xi}_{n-1} \cdot \boldsymbol{n} \qquad \square$$

Hence, the proposed discretisation automatically preserves the control angular momentum whenever the mechanical system has rotational symmetry.